

Article

Pixel-Based Spatio-Statistical Analysis of Landslide Probability in Humid and Seismically Active Areas of Himalaya and Hindukush

Sajjad Muhammad Khan ^{1,*}, Atta-Ur Rahman ², Muhammad Ali ¹, Fahad Alshehri ³,
Muhammad Shahab ^{3,*} and Sajid Ullah ³

¹ National Centre of Excellence in Geology, University of Peshawar, Peshawar 25130, Pakistan; aliumarzai@uop.edu.pk

² Department of Geography and Geomatics, University of Peshawar, Peshawar 25120, Pakistan; atta-ur-rehman@uop.edu.pk

³ Abdullah Alrushaid Chair for Earth Science Remote Sensing Research, Geology and Geophysics Department, College of Science, King Saud University, P.O. Box 2455, Riyadh 11451, Saudi Arabia; falshehria@ksu.edu.sa (F.A.); sajidullahgis24@gmail.com (S.U.)

* Correspondence: syed.sajjadmuhammad@uop.edu.pk (S.M.K.); shahabgeo07@gmail.com (M.S.)

Abstract: The Hindukush and Himalaya regions of Pakistan are chronically prone to several geological hazards such as landslides. Studying landslides in these regions is crucial for risk assessment and disaster management, as well as for determining the effects of adverse climatic conditions, infrastructure management, and increasing anthropogenic activities. High-relief mountains in these regions face severe challenges because of frequently occurring landslides and other natural hazards, especially during intensive rainfall seasons and seismic activity, which destroy infrastructure and cause injuries and deaths. Landslides in the Alpuri Valley (Hindukush) and the Neelum Valley (Himalaya) have been activated through high magnitude earthquakes, intensive rainfalls, snowfall, floods, and man-made activities. Landslide susceptibility mapping in these areas is essential for sustainable development as it enables proactive risk management, up-to-date decision-making, and effective responses to landslide hazards, ultimately safeguarding human lives, property, and the environment. In this study, the relative effect method was applied for landslide susceptibility modeling in both study areas to determine the capability to reduce the effects of landslides, and to improve the prediction accuracy of the method. The relative effect is a statistical model that has only been used for very limited time for landslide susceptibility with effective results. A total of 368 (Neelum Valley) and 89 (Alpuri Valley) landslide locations were identified, which were utilized to prepare the reliable landslide inventory using GIS. In order to evaluate the areas at risk for future landslides activities and determine their spatial relationship with landslide occurrences, the landslide inventory was developed with 17 landslide causative factors. These factors include slope gradient, slope aspect, geology, plan curvature, general curvature, profile curvature, elevation, stream power index, drainage density, terrain roughness index, distance from the roads, distance from the streams, distance from fault lines, normalized difference wetness index, land-use/land-cover, rainfall, and normalized difference vegetation index. Finally, the performance of the relative effect method was validated using the success and prediction curve rate. The AUC-validated result of the success rate curve in the Alpuri Valley is 74.75%, and 82.15% in the Neelum Valley, whereas, the AUC-validated result of the prediction rate curve of the model is 87.87% in the Alpuri Valley and 82.73% in the Neelum Valley. These results indicate the reliability of the model to produce a landslide susceptibility map, and apply it to other landslide areas. The model demonstrated a more effective result in the Alpuri Valley, having a smaller area. However, the results are also desirable and favorable in Neelum Valley, with it being a large area. It will assist in general landslide hazard management and mitigation, and further research studies related to future landslide susceptibility assessments in other parts of the region.

Keywords: relative effect model; Neelum Valley; Alpuri Valley; landslide susceptibility mapping; remote sensing; GIS; sustainable development



Citation: Khan, S.M.; Rahman, A.-U.; Ali, M.; Alshehri, F.; Shahab, M.; Ullah, S. Pixel-Based Spatio-Statistical Analysis of Landslide Probability in Humid and Seismically Active Areas of Himalaya and Hindukush. *Sustainability* **2024**, *16*, 3556. <https://doi.org/10.3390/su16093556>

Academic Editor: Lucio Di Matteo

Received: 29 December 2023

Revised: 31 March 2024

Accepted: 7 April 2024

Published: 24 April 2024



Copyright: © 2024 by the authors. Licensee MDPI, Basel, Switzerland. This article is an open access article distributed under the terms and conditions of the Creative Commons Attribution (CC BY) license (<https://creativecommons.org/licenses/by/4.0/>).

1. Introduction

A landslide is the most terrible natural hazard globally, occurring in mountainous regions [1,2]. The rapid development of infrastructure in mountainous regions, increased human activity, and global climatic changes have increased the trend and frequency of landslides [3]. Landslide events cause the loss of human life and billions of dollars in property damages every year [1]. Globally, the number of human casualties due to landslide events was 4800 from 2004 to 2016 [4]. Planning and management are very necessary to protect areas from landslide hazards in future.

Landslide events are frequent in the mountain ranges of northern Pakistan. These mountain ranges have rough terrain, weak geology, steep slopes, high elevation, deforestation, soil cohesion, precipitation, variation in climatic conditions, infrastructure on unstable slopes, and seismic activities, which all make the area increasingly prone to landslides.

Remote sensing data, such as air photographs and satellites images with their spatial resolution, coverage of the area from time to time, and ease of acquisition, are more effectively used in landslide monitoring and analysis from local to regional scales [5–8]. A landslide inventory, acquired from satellite images and air photos, is utilized for landslide hazard, vulnerability, and risk assessment. It also plays a role in the rapid appraisal of the distribution and intensity of landslides, as well as for landslide susceptibility mapping [9]. This mapping is used for future planning and mitigation of the effects of landslide occurrence. Quantitative, qualitative, and semi-quantitative methods have been utilized in landslide susceptibility mapping in a GIS environment [10].

This research evaluated where landslides are likely to occur through landslide susceptibility mapping of the Alpuri Valley and the Neelum Valley [11], and was prepared using the relative effect method. It is a quantitative model, mathematically establishing the relation of landslide occurrence with various causative factors [12]. Results of the area under the curve were compared to determine the model's suitability, accuracy, and performance in different valleys. The Alpuri and Neelum Valleys have different characteristics. The area of the Alpuri Valley is one-third of the Neelum Valley. Due to the variation in area, the effectiveness of the relative effect method varied equally in the valleys. This variation indicates the applicability, suitability, and plausibility of the model.

2. Study Area

Two high-relief mountain regions in northern Pakistan, the Alpuri Valley and the Neelum Valley, were selected for landslide susceptibility mapping in this study (Figure 1). The Alpuri Valley is part of the Hindukush mountain range (District Shangla of Khyber Pakhtunkhwa province), while the Neelum Valley is located in the Himalaya mountain range (largest district of Azad Kashmir). These mountain ranges are seismically and tectonically active. The Alpuri Valley is bounded by latitude 34–35° N and longitude 72–73° E, and the Neelum Valley is bounded by latitude 32–35° N and 73–75° E. Approximately, the Alpuri Valley covers an area of 812 Km², while the Neelum Valley covers an area of 3737 Km². The altitude of the Alpuri Valley and the Neelum Valley is 1471 m and 4700 m above mean sea level, respectively. The annual precipitation rate in the Alpuri Valley and the Neelum Valley is 1600 mm and 1650 mm, respectively [13]. The climate of the Alpuri Valley is humid to sub-humid zone, whereas in the Neelum Valley, the climate is sub-humid. Valleys in the region are filled with thick layers of unconsolidated lacustrine, glacial, and fluvial deposits. The rugged topography with steep mountain slopes contains loose material, and the valley floor produces a high rate of erosion by the river and its tributaries. Various factors in these valleys, such as active tectonics, anthropogenic factors, high erosion process, and rugged topography, make them prone to various types of geohazards, particularly landslides. Both valleys are famous for their scenic beauty and tourism. They are blessed with natural resources including precious minerals and forests.

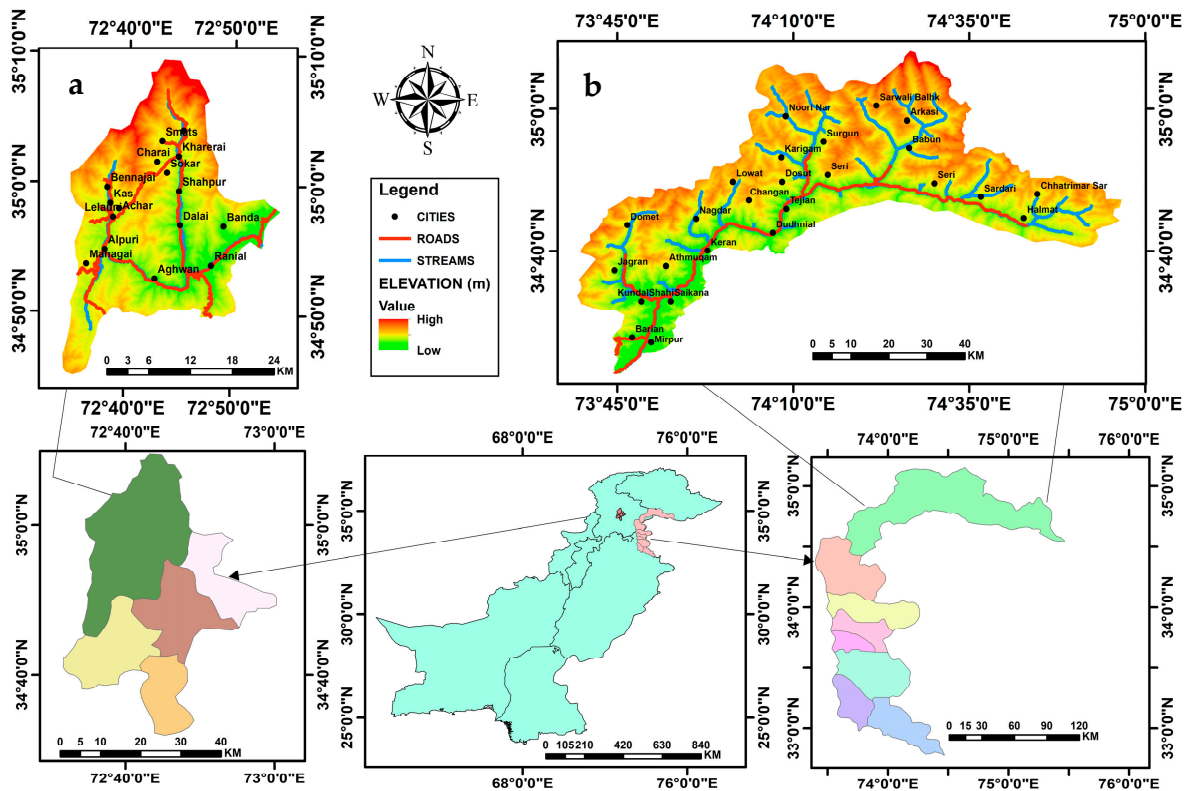


Figure 1. The study areas (a) Alpuri Valley and (b) Neelum Valley.

3. Materials and Methods

In this study, quantitative assessment of landslide susceptibility was evaluated through the relative effect model, using 17 landslide causative factors. These factors include slope gradient, elevation, profile curvature, plan curvature, slope aspect, SPI, drainage density, TRI, NDWI, NDVI, general curvature, geology, distance from roads, distance from fault lines, LULC, rainfall, and distance from streams for landslides. Different reliable sources were used to collect the required data for landslide susceptibility (Table 1). Geological maps of northern Pakistan, fault lines maps of the study areas, Google Earth images, ALOSPALSAR digital elevation model, global precipitation measurement mission rainfall data, topographic maps, Sentinel-2 satellite images, and Sentinel-2 land-use land-cover maps were utilized in this study. Field surveys were conducted to evaluate the landslide causative factors and map the past landslides in study areas. Remotely sensed data in GIS environment were used to develop the landslide inventory and causative factors maps.

Table 1. Data used for landslide susceptibility model.

Landslide Inventory	Field Data and Satellite Images	Scale	Polygons and Points
Lithology	Geological map	1:50,000	Lithological units
Slope gradient	ALOSPALSAR DEM	12.5 m	Natural break
Slope aspect	ALOSPALSARDEM	12.5 m	Natural break
Elevation	ALOSPALSAR DEM	12.5 m	Natural break
General curvature	ALOSPALSAR DEM	12.5 m	Natural break
Profile curvature	ALOSPALSAR DEM	12.5 m	Natural break
Plan curvature	ALOSPALSAR DEM	12.5 m	Natural break
TRI	ALOSPALSARDEM	12.5 m	Natural break
SPI	ALOSPALSAR DEM	12.5 m	Natural break
Distance to streams	ALOSPALSAR DEM	12.5 m	Natural break

Table 1. Cont.

Landslide Inventory	Field Data and Satellite Images	Scale	Polygons and Points
Drainage density	ALOSPALSAR DEM	12.5 m	Natural break
Distance to roads	Topographic map	1:50,000	Natural break
NDVI	Sentinel 2	10 m	Natural break
NDWI	Sentinel 2	10 m	Natural break
Land-use, land-cover	Sentinel 2	10 m	Natural break
Distance from faults	Geological map	1:50,000	Natural break
Rainfall (mm)	GPM	30 m	Natural break

3.1. Data Preparation

For mapping the susceptibility to landslides, a variety of geomorphological, geological, hydrological, proximity, and triggering elements were coupled with other landslide causative components. Slope aspect, slope gradient, profile curvature, elevation, plan curvature, general curvature, land-use, land-cover, and TRI were included as geomorphological factors. The surface geology of the study area was incorporated as a geological factor. The hydrological parameters included drainage density, SPI, and rainfall. Distance from streams, roads, and fault lines were utilized as proximity factors while NDVI and NDWI were also included (Table 1). The criteria for including these factors was based on the past landslide information and their contribution to the likelihood of landslide occurrences in future. All these various causative factor maps were organized in the raster format with a cell size of 12.5×12.5 m.

The methodology of this research study started from past landslide inventory. Field surveys, Google Earth, and sentinel satellite images were used to prepare the historical landslide inventory. A total of 89 landslides were mapped in the Alpuri Valley and 368 landslides were mapped in the Neelum Valley (Figure 2). These landslides were digitized in the ArcGIS application and overlaid on the sentinel images to evaluate the accuracy of landslide areas/location. Detailed field surveys were carried out to verify the accuracy of the landslide inventory. These landslides were converted to raster format with 12.5 by 12.5 m spatial resolution. The landslide inventory was divided in two parts for the validation process of the model: a 70% ratio for training data and a 30% ratio testing data.

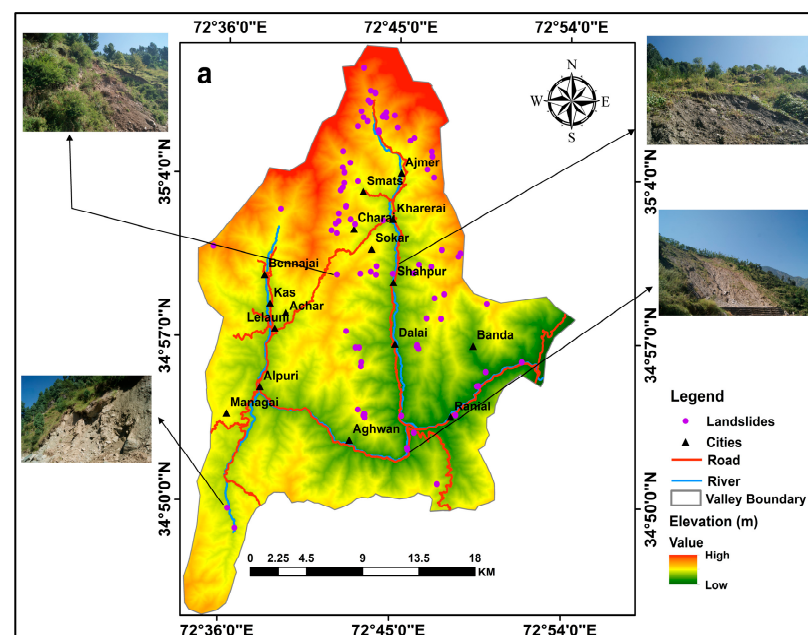


Figure 2. Cont.

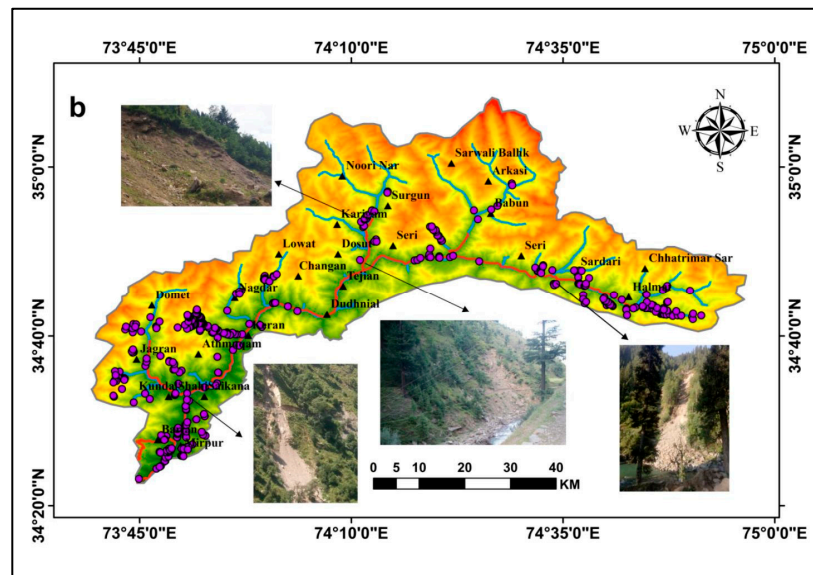


Figure 2. Spatial distribution of landslide types of (a) Alpuri Valley (b) Neelum Valley.

3.2. Geomorphological Factors

3.2.1. Slope Gradient

Slope gradient is one of the direct influencing factors of landslides, and has a close relationship with the landslides. The density of landslides increases with an increase in slope angle [14]. It has been identified that the frequency of landslides increases with changing the slope gradient from low to high. However, there is a higher concentration of landslides at the medium slope gradients as compared to gentle and high slope gradients [15]. Characteristics of slope define the relief characteristics and terrain stability. Many studies indicate that the slope factor has a great impact on landslide susceptibility analysis [16,17]. In this study, the ALOSPALSAR DEM has been utilized for extracting the slope gradient of study regions (Figures 3a and 4a). Slope gradient maps were classified into five classes using the natural break technique.

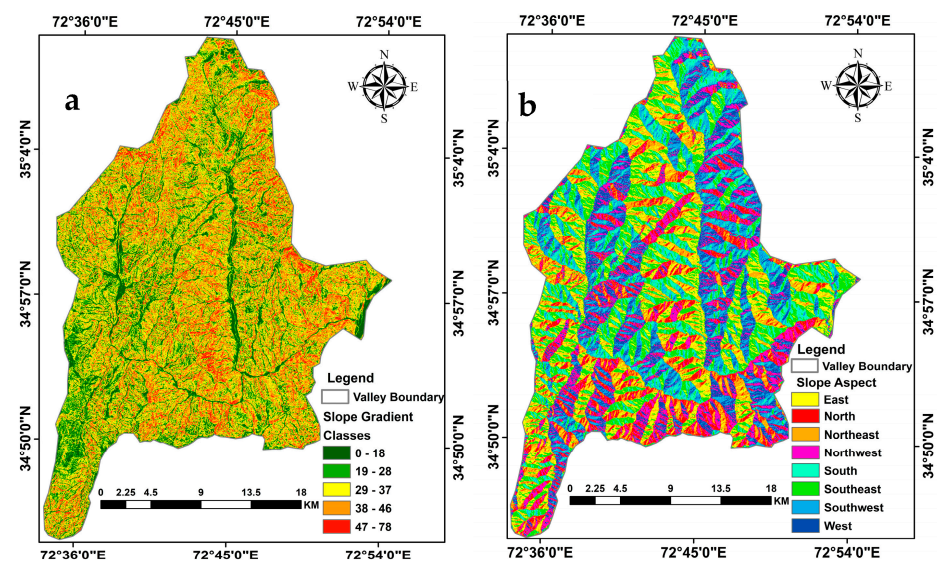


Figure 3. Cont.

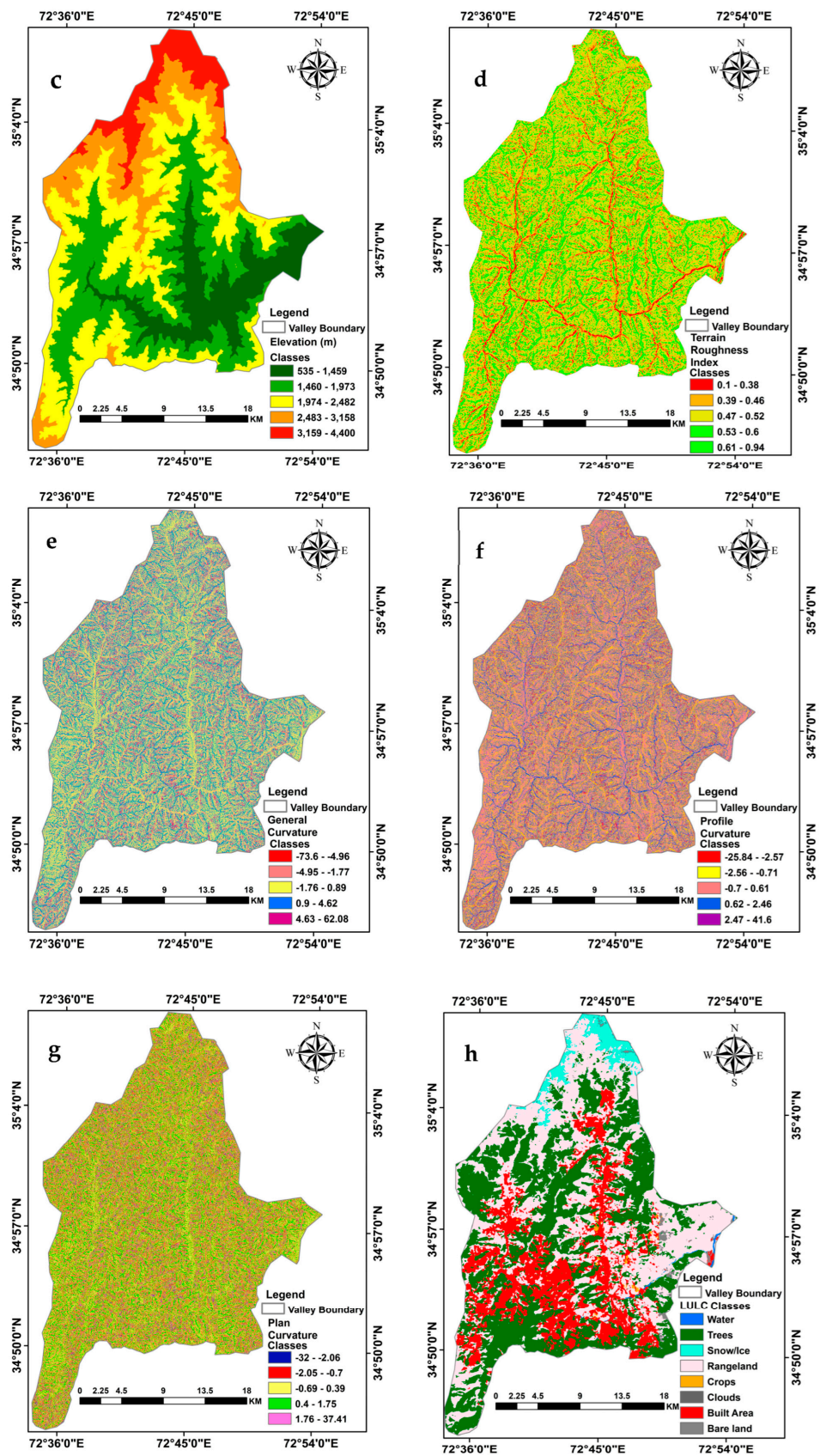


Figure 3. Cont.

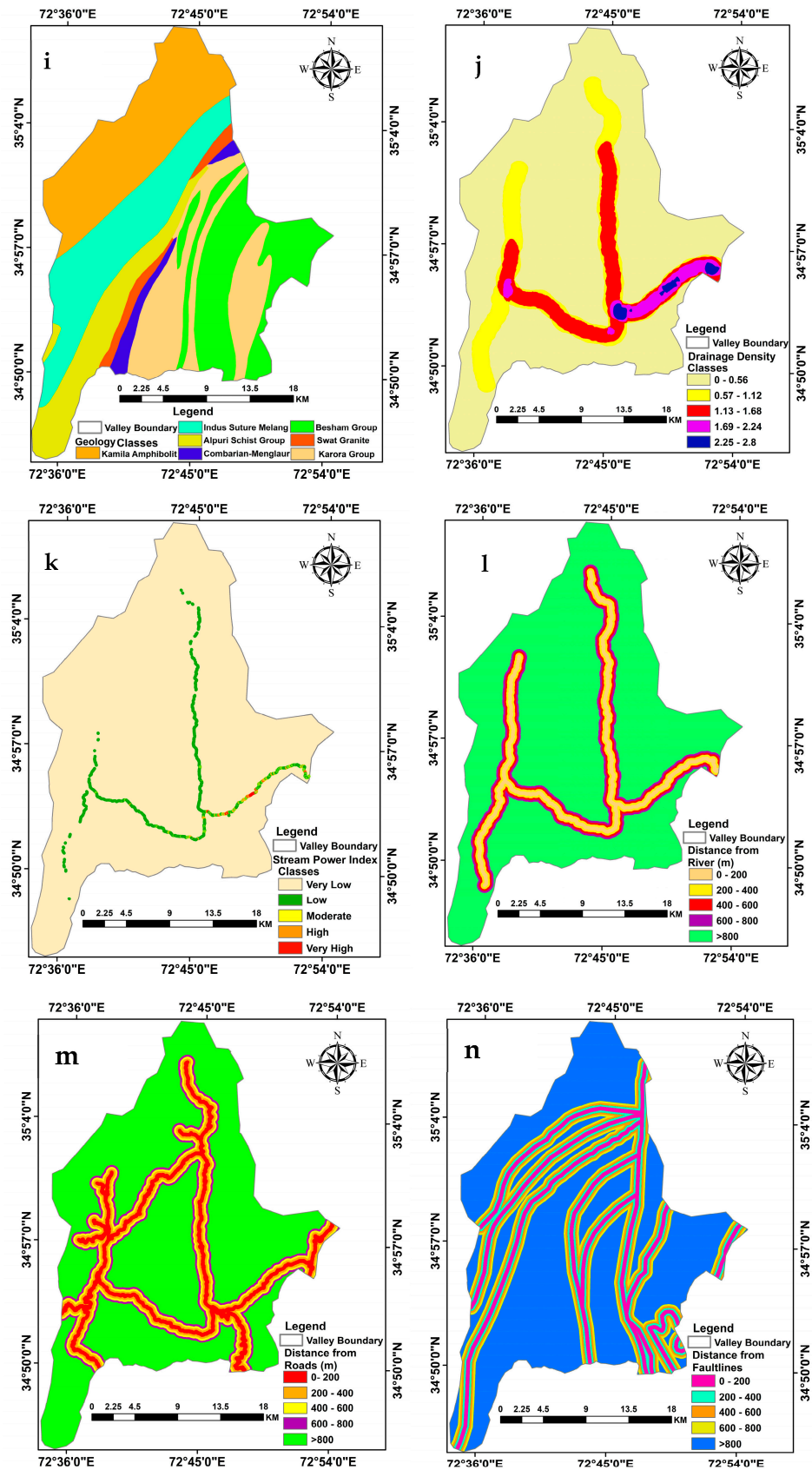


Figure 3. Cont.

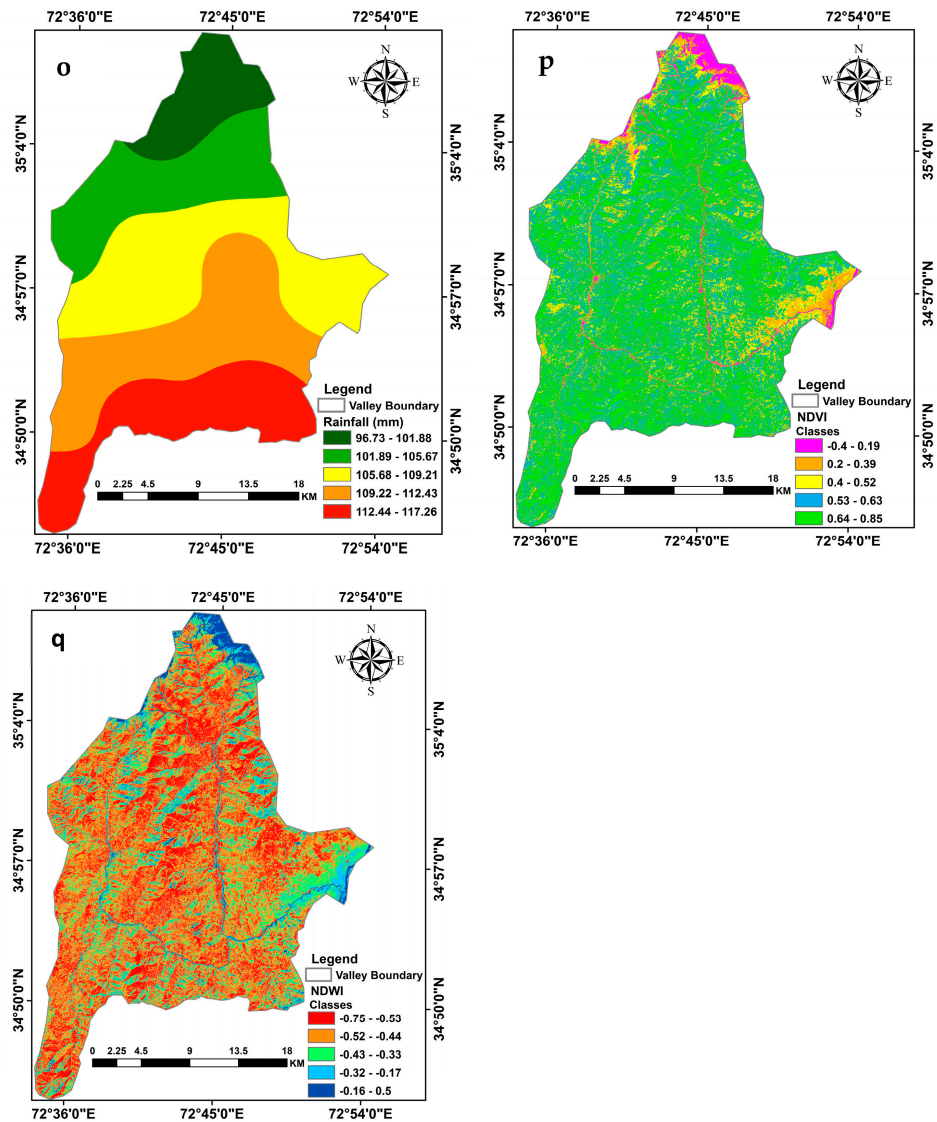


Figure 3. Thematic maps of the Alpuri Valley: (a) slope gradient; (b) slope aspect; (c) elevation; (d) terrain roughness index; (e) general curvature; (f) profile curvature; (g) plan curvature; (h) land-use land-cover; (i) geology; (j) drainage density; (k) stream power index; (l) distance from road; (m) distance to river; (n) distance from fault lines; (o) rainfall data; (p) NDVI; (q) NDWI.

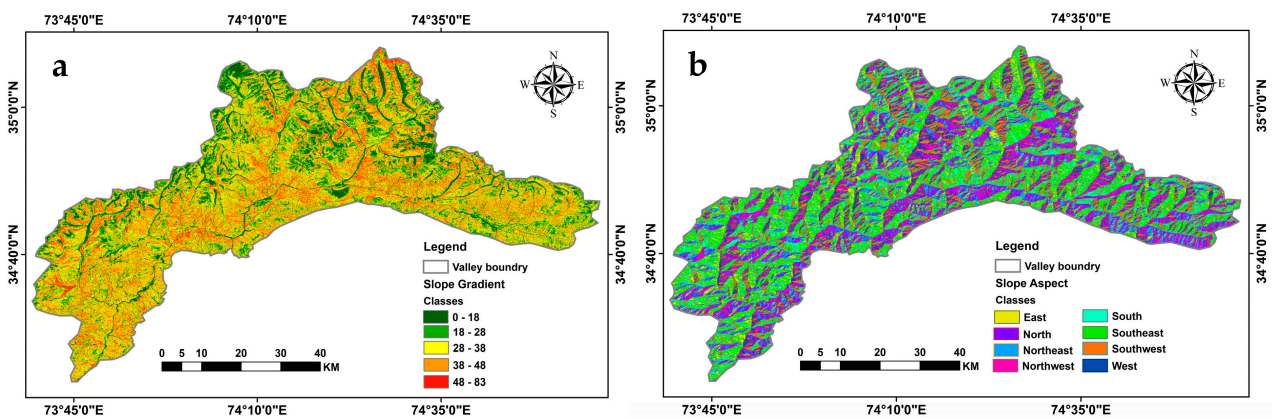


Figure 4. Cont.

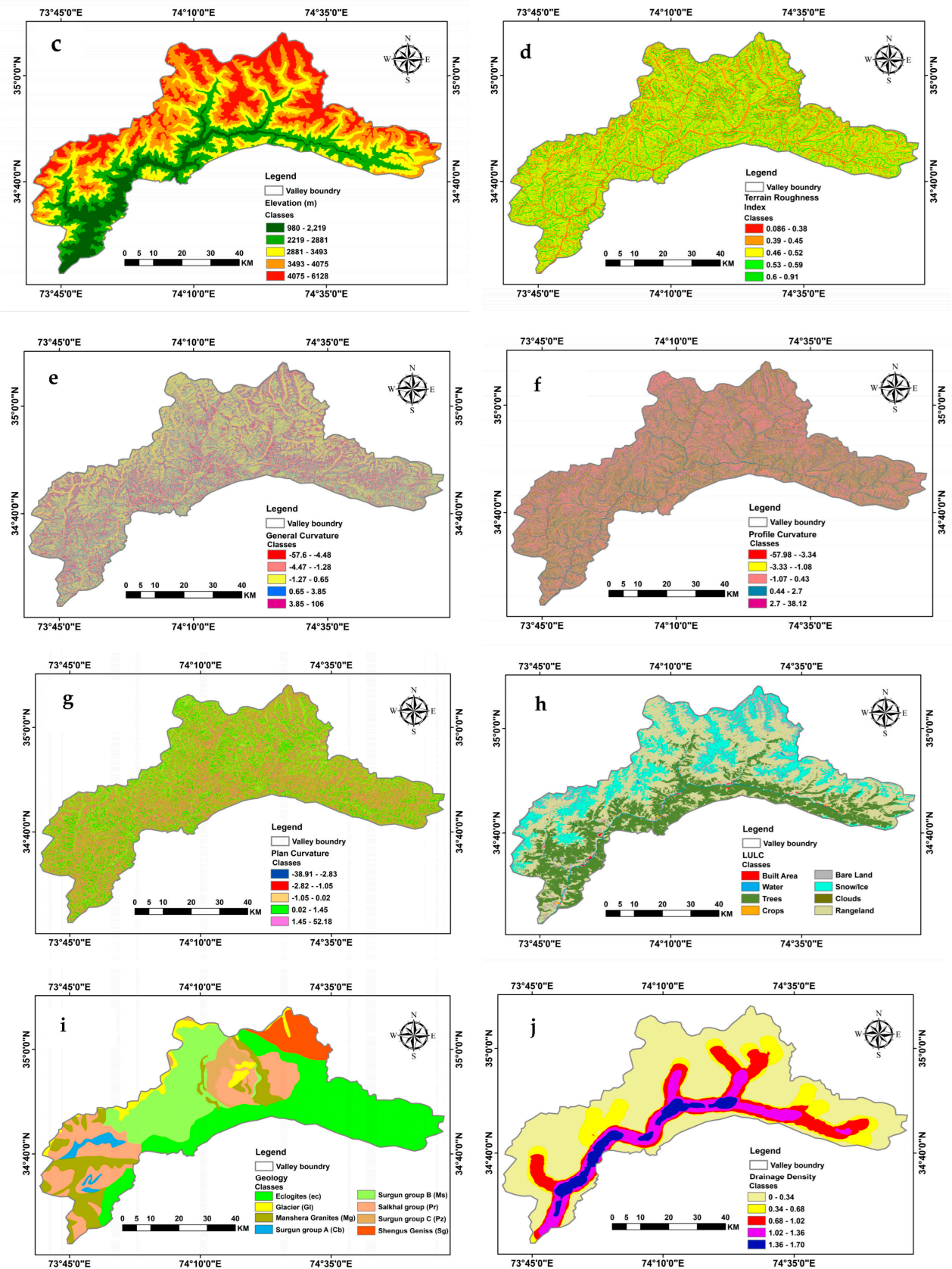


Figure 4. Cont.

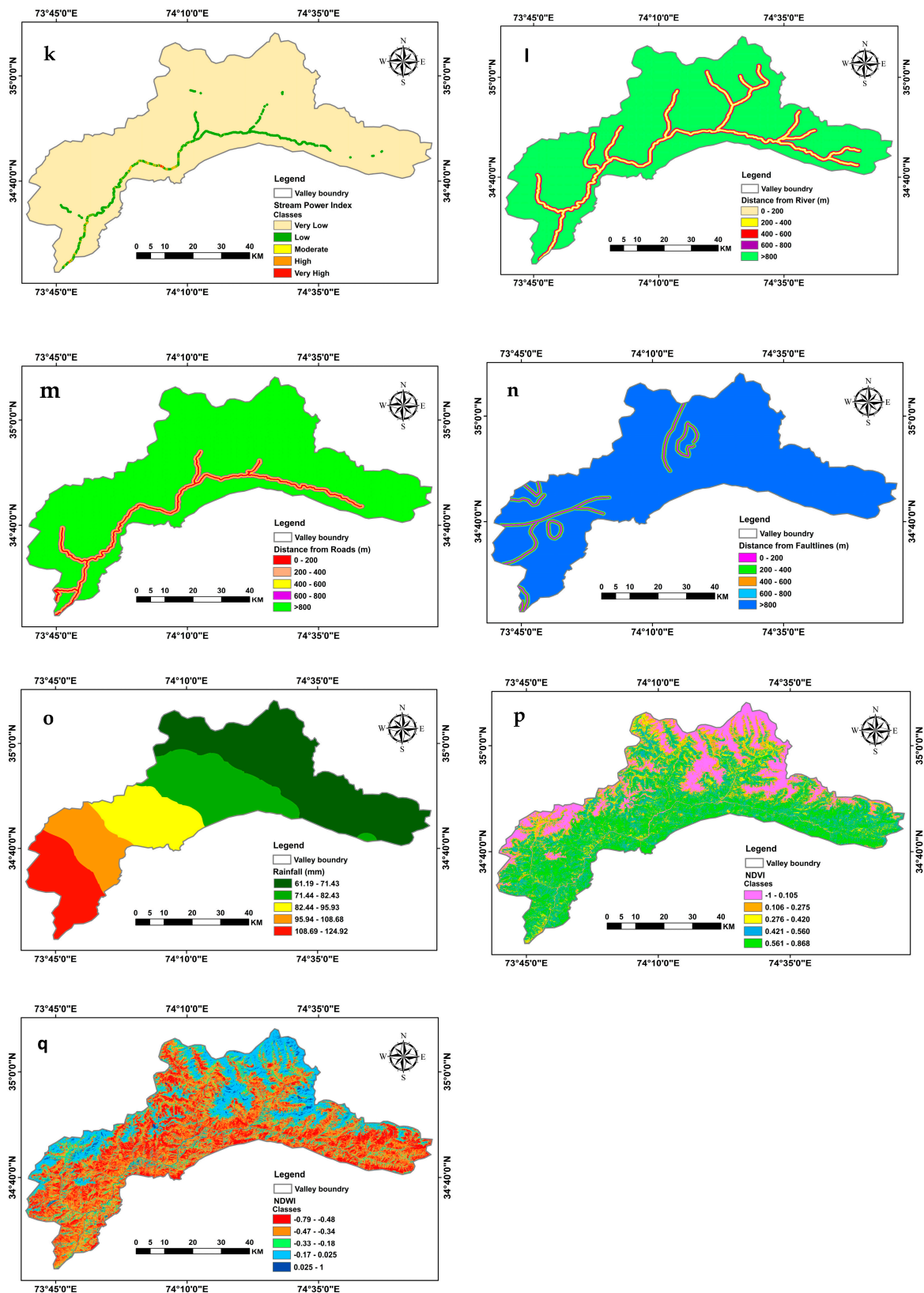


Figure 4. Thematic maps of the Neelum Valley: (a) slope gradient; (b) slope aspect; (c) elevation; (d) terrain roughness index; (e) general curvature; (f) profile curvature; (g) plan curvature; (h) land-use land-cover; (i) geology; (j) drainage density; (k) stream power index; (l) distance from road; (m) distance to river; (n) distance from fault lines; (o) rainfall data; (p) NDVI; (q) NDWI.

3.2.2. Slope Aspect

The slope aspect consists of 8 directions of slope with respect to landslide occurrence. These directions are north, northeast, east, southeast, south, southwest, west, and northwest. These directions are based on 0–360 degrees in a clockwise direction. It is an important factor in landslide susceptibility mapping [18] as every slope aspect has obvious impact on landslide occurrences. It plays a passive role in topographic factors and has an indirect impact on the landslide events. ALOSPALSAR DEM was utilized to extract the slope aspect factor for landslide susceptibility assessment (Figures 3b and 4b).

3.2.3. Elevation

Elevation is the height of a point above mean sea level, and is a direct influencing factor of landslide events. Rock weathering processes are carried out on the basis of elevation [19]. Higher elevation increases weathering processes, which represent weak geological units, and, hence, a high tendency for landslides is found [20]. ALOSPALSAR DEM was utilized to prepare elevation factor and elevation of the study regions was classified into five classes (Figures 3c and 4c).

3.2.4. Terrain Roughness Index (TRI)

Terrain roughness index (TRI) is the calculation of difference between the maximum point and minimum point of local terrain [21]. It represents the elevation difference of a point with respect to its surrounding area, and works as a significant morphological factor in landslide occurrence and landslide susceptibility mapping [22]. It also determines the changes in relief and degree of erosion. The following Equation (1) is used to calculate the TRI:

$$TRI = \sqrt{|x|(\max^2 - \min^2)} \quad (1)$$

TRI is the terrain roughness index, max is the maximum point, and min is the minimum point [23]. Raster calculator tool in ArcGIS 10.7 software was utilized to calculate the terrain roughness index (Figures 3d and 4d).

3.2.5. General Curvature

Curvature is the morphological factor of landslide occurrence. In previous studies, it was utilized for landslide susceptibility assessment. It defines the change in slope gradient with respect to the morphology of the ground surface [24,25]. Mathematically, it is defined as the rate of change in slope degree with the parallel of the small arc of the curve [26]. It determines the effect of slope material and water flow [27,28]. There are an infinite number of curvature values that exist in a hill slope region. There are three curvature sides used in hillslope and landslide analysis. General curvature data were also derived from the ALOSPALSAR DEM, and classified into five classes (Figures 3e and 4e).

3.2.6. Profile Curvature

Profile curvature is the curvature along with the vertical position of topography and slope orientation. It divides the hillslope into concave, convex, and flat (neutral) classes. The concave class is a region where the water flow converges [29,30], whereas the convex class contains the water flow divergence [29]. It is the inverse of plan curvature. Every sub-region is identified according to its values. A concave area has negative values and a high possibility of landslide occurrence, whereas a convex area has positive values and a flat area has zero values. Profile curvature influences the pressure and force within the landslide toward the direction of motion. ALOSPALSAR DEM was utilized to extract profile curvature and was classified into five classes using the natural break (Figures 3f and 4f).

3.2.7. Plan Curvature

Plan curvature is the line of curvature along the horizontal plane of topography and perpendicular to the slope direction. It controls both convergence and divergence of

landslide materials and water flow in landslide orientation [31]. Concave, convex, and flat are the sub-regions of hillslope of plane curvature. The concave area has positive values and the convex region has negative values. The flat area has zero values. ALOSPALSAR DEM was used to extract the plan curvature factor (Figures 3g and 4g).

3.2.8. Land-Use Land-Cover (LULC)

Land-use land-cover (LULC) is another potential factor of landslide susceptibility, which shows the natural process as well as the anthropogenic process. Vegetation is a significant class of LULC with a strong and extensive rooting system, which increase the slope stability through its effect on the soil's hydrological and mechanical attributes [32,33]. In this study, various classes of LULC were extracted from the Sentinel-2 land-use land-cover image and reclassified into eight classes (Figures 3h and 4h). These classes included crops, bare land, clouds, snow/ice, rangeland, built area, water, and trees.

3.3. Geological Factor (Surface Geology)

Surface geology has strong connectivity with landslide events and landslide susceptibility mapping [32]. Weak and undeveloped geological structures act as an effective factor of geology for more landslide-prone areas. Characteristics of slope materials such as permeability, strength, rock types, and weathering activities are responsible factors for slope failure. Geology of the northern mountainous region started at the time of the collision of the Indo-Australian plate with the Eurasian Plate. The mountainous region of Pakistan is the youngest mountain system, initiated in the Cretaceous to Mio-Pliocene age [34]. The geological information of study areas was derived from geological maps of northern Pakistan (Figures 3i and 4i). Geologically, these valleys are fragile and have immature mountainous regions and mostly sedimentary rock, which makes them more susceptible to landslides. Lithology units of the Alpuri Valley are Kamila amphibolite complex (Ka), Swat granites (Swg), Indus suture mélange (Ism), Karora group (Pr), Cambrian Manglaur formation (Cb), Alpuri group–Alpuri schist (Ms), and the Besham formation (A). The lithological units of the Neelum Valley are eclogites (ec), Shengus gneiss (Sg), Manshera granites (Mg), glacier (Gi), Surgun group-C (Pz), Sugun group-B (Ms), Surgun group-A (Cb), and the Salkhala group (Pr).

3.4. Hydrological Factors

3.4.1. Drainage Density

Drainage density is defined as the ratio of total stream length to the total area of a drainage basin. It depends on flow of water in streams at the surface. Landslides arise as a result of erosion processes brought on by runoff water and eroded material flow in streams in mountainous areas [35]. Drainage density is the quantitative value that expresses that a higher value indicates a low infiltration rate and high rate of runoff. Equation (2) is utilized for drainage density [36]:

$$DD = \left(\frac{LS}{AD} \right) \quad (2)$$

where DD is the drainage density, LS is the total length of streams, and AD is the total area of the drainage basin of the study area. Drainage density map was classified into five classes of the study areas (Figures 3j and 4j).

3.4.2. Stream Power Index (SPI)

Stream power index is a hydrological factor used to measure the erosion power ability of water, based on the theory that discharge is directly proportional to catchment area [37]. It represents the direct relation between the erosion power of water and slope. Stream power index was calculated using Equation (3);

$$SPI = A \tan \beta / b \quad (3)$$

where A is the catchment area and b is the degree of slope. Higher value of SPI represents the high possibility of erosion power [38].

Stream power index was prepared using the ALOS PALSAR DEM and was classified into five classes (Figures 3k and 4k). Every class of factor has its effect on landslide occurrence. According to the relative effect model, a positive value represents the high possibility of landslide events and a negative value determines a low or no possibility of landslide occurrence.

3.5. Proximity Factors

3.5.1. Distance from Roads

Roads are also an important anthropogenic parameter in landslide occurrence in mountainous areas [39,40]. Roads play a role in the changing of slope gradient [41,42]. In hilly areas, the roads are mostly constructed at the toe part of the hill and a few meters above the river. Road construction, its expansion, and heavy vehicles may affect the slope stability and force the landslide occurrences [43]. The roads were considered as potential triggering factor and associated with a probability of landslide occurrence. Topographic sheets of the study areas were utilized to digitize the road networks of the study areas. Multiple buffer tool with 200 m intervals was used to prepare the distance from the roads and classified into five buffer classes from 0 to >800 (Figures 3l and 4l).

3.5.2. Distance from River

Rivers change the topography of the land and contribute to erosion through the fluvial cycle [44]. Runoff water from the river regularly causes erosion and undercutting, which enhances the power of devastation by raising the slope gradient and increasing the likelihood of landslides around the river. The power of the erosion process is high near the river, which indicates a high possibility of landslide events [45]. The area around the river was classified into five classes with an interval of 200 m (Figures 3m and 4m).

3.5.3. Distance from Fault Line

The primary factor leading to slope instability is the movement along faults, which triggers new landslides and reactivates the older ones [46,47]. Some studies suggest that a reduction in distance to faults raises the probability of landslide occurrence [48]. Proximity to faults plays a crucial role in shaping mass movements by impacting surface structures. The proximity to tectonic structures increases the likelihood of landslide occurrences, as erosion processes and water flow along a fissure may take place. In the study areas, fault lines were identified on the geological map and various distance zones were prepared with intervals of 200 m, resulting in the division of the area into five distinct classes. (Figures 3n and 4n). Chakersar fault zone, main mantle thrust, Makhad thrust, Alpuri fault, Puran fault, Karshut fault, Pir sar fault, Besham fault, and Babai thrust belong to the Alpuri Valley. The main central thrust, Shikar fault, structural dome, Richmori fault, Punjal thrust, main boundary thrust, Ganja dome, Gumot shear zone, and Chathic wall fault are located in the Neelum Valley.

3.6. Triggering Factor (Rainfall Data)

Rainfall is an external and temporal triggering factor that plays a significant role in landslide occurrence. In case extreme rainfall events, the slope moves downward as a result of an increase in the pressure of pore water. Rainfall distribution has an impact on soil moisture content and overland flow volume. In this study, the global precipitation measurement (GPM) mission rainfall data were used. Rainfall was spatially distributed based on its mean annual values. Rainfall was reclassified into five classes (Figures 3o and 4o).

3.7. Other Factors

3.7.1. Normalize Difference Vegetation Index (NDVI)

Normalize difference vegetation index is utilized for calculating the presence and absence of vegetation in an area. The index is based on the near-infrared and red wavelength bands of satellite images. The presence of dense vegetation determines the high cohesion power in soil, which decreases the soil erosion process and, hence, landslides occurrence is low. If the concentration of vegetation is low, then the concentration of landslide occurrence is high due to the high rate of soil erosion processes and low cohesion power in soil. This index formulates as Equation (4):

$$\text{NDVI} = \frac{\text{NIR} - \text{RED}}{\text{NIR} + \text{RED}} \quad (4)$$

where NDVI shows normalized difference vegetation index, NIR is the near infra-red band, and RED is a red band of the satellite image. The scale of NDVI is between -1 to $+1$. The -1 value represents an absence of vegetation and the $+1$ value represents very dense vegetation. In the Alpuri and Neelum Valleys, the Sentinel-2 satellite images with 10 m spatial resolution were used to prepare the NDVI maps (Figures 3p and 4p). These maps were classified into five classes.

3.7.2. Normalize Difference Water Index (NDWI)

McFeeters introduced the normalize difference water index in 1996. Water bodies are identified that are associated with wetlands [49]. This index is calculated through the green wavelength band and near-infrared wavelength band of the satellite image. Equation (5) was employed, as given below:

$$\text{NDWI} = \frac{(\text{GREEN} - \text{NIR})}{(\text{GREEN} + \text{NIR})} \quad (5)$$

If the value of NDWI is greater than zero, it identifies water bodies and if NDWI value is less than zero, it represents non-water bodies. NDWI map was also prepared from the Sentinel 2 satellite image and classified into five classes (Figures 3q and 4q). Each class of NDWI calculates the relative effect value. These values determined the ratio of landslide occurrence in each class.

3.8. Application of Relative Effect Method

Relative effect model is a logarithmic-based statistical model (Equation (6)) that is utilized to find out the correlation of each landslide causative factor with distribution of landslides in the study areas. It is introducing a function called relative function (RF). These spatial correlations indicate the effect of landslides in each class of individual factors. Equation (7) shows the ratio of landslide area (sld) in the unit area as per total area of landslide (SLD) and in Equation (8), 'a' shows the ratio of unit area in the entire area of the study (A) for every unit.

$$\text{RE} = \text{Log} \left(\frac{\text{SR}}{\text{AR}} + \epsilon \right) \quad (6)$$

$$\text{SR} = \frac{\text{sld}}{\text{SLD}} \quad (7)$$

$$\text{AR} = \frac{a}{A} \quad (8)$$

RE shows the relative effect, 'SLD' indicates the total number of landslide pixels in the unit area, 'sld' indicates the total number of landslide pixels in each unit, 'a' represents the total number of pixels in a unit, and 'A' indicates the total number of pixels in a unit area. Epsilon (ϵ) shows a very small floating value near zero.

In the relationship's analysis, three cases listed below are used for calculating the relative effect of each class depending on its RE values.

The first case shows the positive effect, meaning if the value is greater than zero, this means the landslide ratio is greater than its unit ratio. This case shows the increasing effect of landslide susceptibility.

The second case shows the negative effect when the value is less than zero, which means the landslide ratio is less than the unit ratio. This case shows the decreasing effect of landslide susceptibility.

The third case shows the zero effect, when the value is equal to zero, which means the landslide ratio is equal to the unit ratio, which represents no effect of landslide susceptibility.

Finally, the landslide susceptibility index (LSI) is calculated using Equation (9):

$$LSI = \sum RE \quad (9)$$

All of the 17 selected factors maps were integrated using the values of relative effect to predict the landslide susceptibility index. This index was finally developed in the landslide susceptibility zonation maps, which were classified into four zones. Every zone describes the level of landslide susceptibility.

4. Results

Landslides are severe problems in mountainous regions of the world. Pakistan is prone to earthquakes and landslides, as a major part of the country is comprised of mountains. Weak, fragile, and immature geological structures in these mountains cause landslides. Proper planning and management are essential to mitigate the effects and intensity of landslides, and prevent the area from experiencing landslides in future. Landslide susceptibility mapping is the primary step for this purpose. A relative effect model was utilized to generate the landslide susceptibility map. This logarithmic model indicated the landslide-affected areas and determined the relationship between causative factors and landslide distribution.

4.1. Landslide Inventory

A total of 368 and 89 landslides were identified and mapped in an area of 7.283 km² and 0.465 km² to reflect the landslide inventory of the Neelum and Alpuri Valleys (Table 2 and Figure 5). The majority of the landslides were slides but debris flows covered a larger area than the slides. In the study areas, slides were found to be the dominant type of landslide (Table 2 and Figure 5). The total number of slides were 240 (65.22%) and 57 (64.05%) in the Neelum and Alpuri Valleys, respectively. The largest mapped slide in the areas has an area of 0.326 and 0.023 km² while the smallest has an area of 0.0002 and 0.0001 km². Most of them were observed along the roads and streams of the study areas.

Table 2. Landslide inventories in the study areas.

Landslides in Alpuri Valley					Landslides in Neelum Valley				
LS Types	Total LS	LS (%)	LS Area (Km ²)	LS Area (%)	LS Types	Total LS	LS (%)	LS Area (Km ²)	LS Area (%)
Slide	57	64.05	0.224	48.17	Slide	240	65.22	3.47	47.7
Debris flow	31	34.83	0.011	49.46	Debris flow	124	33.70	3.76	51.65
Rock fall	1	1.12	0.230	2.37	Rock fall	4	1.08	0.05	0.68
Total	89	100	0.465	100	Total	368	100	7.28	100

Debris flows are the second most frequently occurring phenomenon in the areas with an area of 3.76 km² (51.65%) and 0.011 km² (49.46%) in the Neelum and Alpuri Valleys, respectively. The total number of observed debris flows were 124 (Neelum Valley) and 31 (Alpuri Valley). In case of the debris flows, the largest mapped landslide in the area was observed with areas of 0.223 km² and 0.281 km² while the smallest mapped landslides

had areas of 0.001 km² and 0.0004 km² in the Neelum and Alpuri Valleys, respectively. During the field surveys, it was noted that debris flow occurred mostly in the vicinity of minor streams and in areas experiencing heavy rainfall. In the study areas, there are four (1.08%) and one (1.12%) rock-fall-type of landslides having an area of 0.05 km² (0.68%) and 0.23 km² (2.37%) among the total mapped landslides in the Neelum and Alpuri Valleys, respectively. The rock falls were found near the roads in the study areas.

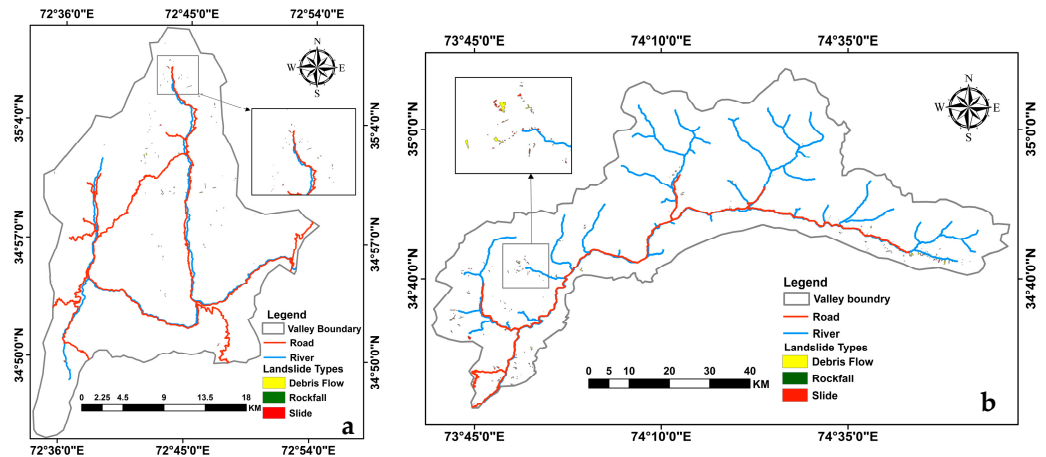


Figure 5. Landslide inventory map of (a) Alpuri Valley and (b) Neelum Valley.

4.2. Modelling Results of Relative Effect Model

The relative effect model was used to calculate the RE value of the landslide causative factors to understand the landslide causative factors for evolving the susceptibility map of the study areas. As shown in Table 3, the relationship between the landslide causative factors and landslide is evaluated to find out the landslide causative factors RE values by using Equation (6). Figure 6 (Alpuri Valley) and Figure 7 (Neelum Valley) represent the relationship of landslides with the causative factors and relative effect values in a graphical form, in order to clarify the effect of causative factors.

Table 3. Alpuri Valley and Neelum Valley, Relative effect values of the landslide causative factors.

Classes	Alpuri Valley			Classes	Neelum Vally		
	% of Pixels in a Class	% of Landslide Pixels in a Class	RE		% of Pixels in a Class	% of Landslide Pixels in a Class	RE
Geology				Geology			
A (Archean–Besham group)	20	28.59	0.16	Cb (Surgun group A)	1.78	6.34	0.55
Cb (Cambrian Manglaur)	2.52	2.84	0.05	Ec (eclogites)	35.92	34.53	−0.02
Ism (Indus Suture mélange)	20.07	22.19	0.04	Gl (glacier)	4.08	0	0
Ka (Kamila amphibolite complex)	25.14	30.01	0.08	Mg (Manshera granites)	11.39	20.29	0.25
Ms (Alpuri schist)	11.56	7.4	−0.19	Ms (Surgun group B)	19.24	2.81	−0.84
Pr (Karor group)	18.13	8.82	−0.31	Pr (Salkhala group)	18.34	31.69	0.24
Swg (Swat granites)	2.58	0.14	−1.26	Pz (Surgun group C)	3.38	4.35	0.11
Nil	Nil	Nil	Nil	Sg (Shengus gneiss)	5.87	0	0
Slope Gradient				Slope Gradient			
0–18	11.31	9.06	−0.096	0–17	12.32	8.26	−0.17
18–28	23.47	18.97	−0.093	17–28	24.81	22.6	−0.04
28–36	30.89	33.29	0.032	28–38	31.21	33.09	0.03
36–46	24.99	27.88	0.047	38–48	22.78	25.99	0.06
46–78	9.34	10.81	0.064	48–84	8.89	10.05	0.05

Table 3. Cont.

Alpuri Valley				Neelum Vally			
Classes	% of Pixels in a Class	% of Landslide Pixels in a Class	RE	Classes	% of Pixels in a Class	% of Landslide Pixels in a Class	RE
Slope Aspect				Slope Aspect			
North	10.24	8.38	−0.17	North	9.93	14.19	0.31
Northeast	11.05	13.44	0.09	Northeast	10.61	11.77	0.05
East	14.45	19.03	0.12	East	12.4	10.96	−0.05
Southeast	15.84	18.84	0.08	Southeast	15.46	15.21	−0.01
South	12.23	16.14	0.12	South	14.87	15.97	0.03
Southwest	13.05	9.42	−0.14	Southwest	14.71	13.52	−0.04
West	12.38	7.86	−0.2	West	11.94	7.63	−0.19
Northwest	10.74	6.72	−0.2	Northwest	10.07	10.74	0.03
Distance from Road				Distance from Road			
0–200	8.22	20.63	0.4	0–200	2.3	8.71	0.58
200–400	7.06	7.4	0.02	200–400	2.17	7	0.51
400–600	6.52	3.18	−0.31	400–600	2.08	5.64	0.43
600–800	6.13	2.09	−0.47	600–800	2.03	4.33	0.33
>800	72.07	66.71	−0.03	>800	91.43	74.32	−0.09
Distance from River				Distance from River			
0–200	5.17	20.72	0.60	0–200	3.72	16.81	0.65
200–400	5	3.41	−0.17	200–400	3.63	8.13	0.35
400–600	4.89	5.97	0.09	400–600	3.53	7.77	0.34
600–800	4.79	2.89	−0.22	600–800	3.51	7.36	0.32
>800	80.16	67	−0.08	>800	85.61	59.93	−0.15
General Curvature				General Curvature			
−73.6–−4.96	2.02	2.18	0.03	−54.64–−4.48	3.04	5.35	0.25
−4.96–−1.77	17.61	23.47	0.12	−4.48–−1.28	25.87	33.17	0.11
−1.77–0.89	50.3	51.45	0.01	−1.28–0.65	42.65	37.7	−0.05
0.89–4.61	28.07	20.39	−0.14	0.65–3.85	25.26	20.62	−0.09
4.61–6.08	2	2.51	0.1	3.85–106	3.19	3.16	0
Elevation				Elevation			
535–1459	15.42	21.57	0.15	980–2219	10.65	31.06	0.46
1459–1973	30.07	22.9	−0.12	2219–2881	20.46	51.23	0.4
1973–2482	30.96	29.45	−0.02	2881–3493	22.92	17.18	−0.13
2482–3158	16	25.65	0.21	3493–4075	26.22	0.53	−1.7
3158–4400	7.56	0.43	−1.25	4075–6128	19.75	0	0
Plan Curvature				Plan Curvature			
−32–2.06	4.23	5.17	0.09	−38.9–−2.83	1.69	2.9	0.23
−2.06–−0.7	20.02	24.56	0.09	−2.83–−1.04	13.2	18.83	0.15
−0.7–0.39	39.77	41.01	0.01	−1.04–0.03	38.27	37.85	0
0.39–1.75	29.19	23.38	−0.1	0.03–1.45	38.17	32.74	−0.07
1.75–37.40	6.8	5.88	−0.06	1.45–52.18	8.66	7.69	−0.05
Profile Curvature				Profile Curvature			
−25.84–−2.57	3.1	3.18	0.01	−57.98–−3.34	1.75	1.98	0.05
−2.57–−0.72	21.82	16.64	−0.12	−3.34–−1.07	14.09	13.11	−0.03
−0.72–0.6	44.82	43.24	−0.02	−1.07–0.43	49.16	42.11	−0.07
0.60–2.45	26.52	32.48	0.09	0.43–2.7	32.04	37.59	0.07
2.45–41.60	3.74	4.46	0.08	2.7–38.12	2.96	5.22	0.25
Terrain Roughness Index				Terrain Roughness Index			
0.10–0.38	6.62	13.04	0.29	0.08–0.38	6.48	13.94	0.33
0.38–0.46	22.13	22.76	0.01	0.38–0.45	20.8	24.46	0.07
0.46–0.52	35.74	42.58	0.08	0.45–0.51	36.91	33.1	−0.05
0.52–0.59	26.6	16.17	−0.22	0.51–0.59	27.07	22.72	−0.08
0.59–0.95	8.91	5.45	−0.21	0.59–0.90	8.74	5.77	−0.18
NDVI				NDVI			
−0.4–0.18	2.63	11.66	0.65	−1–0.10	17.93	8.58	−0.32
0.18–0.39	7.1	44.71	0.8	0.10–0.27	12.2	31.79	0.42
0.39–0.53	18.84	24.23	0.11	0.27–0.42	18.72	29.6	0.2
0.53–0.62	35.38	13.13	−0.43	0.42–0.56	27.47	20.54	−0.13
0.62–0.86	36.04	6.26	−0.76	0.56–0.87	23.69	9.5	−0.4

Table 3. Cont.

Alpuri Valley				Neelum Vally			
Classes	% of Pixels in a Class	% of Landslide Pixels in a Class	RE	Classes	% of Pixels in a Class	% of Landslide Pixels in a Class	RE
Stream Power Index				Stream Power Index			
0–17,346,033	99.93	99.53	0	0–162,747,343	99.97	99.96	−0.00002
17,346,033–69,384,135	0.05	0.33	0.81	162,747,343–623,864,818	0.02	0.01	−0.4
69,384,135–160,450,813	0.01	0.14	0.99	623,864,818–1,329,103,309	0.01	0.01	0.2
160,450,813–307,892,102	0	0	0	1,329,103,309–2,875,203,075	0	0.02	0.8
307,892,102–55,904,832	0	0	0	2,875,203,075–6,916,762,112	0	0	0
NDWI				NDWI			
−0.74–−0.52	26.57	4.98	−0.73	−0.78–−0.48	27.28	7.12	−0.58
−0.52–0.44	38.76	14.46	−0.43	−0.48–−0.34	32.81	33.89	0.01
0.44–0.33	23.11	27.5	0.08	−0.34–−0.17	17.21	41.5	0.38
0.33–0.17	8.37	41.68	0.7	−0.17–0.02	20.25	16.29	−0.09
0.17–0.51	3.19	11.38	0.55	0.02–1	2.44	1.2	−0.31
Drainage Density				Drainage Density			
0–0.56	81.57	68.14	−0.08	0–0.34	72.59	48.21	−0.18
0.56–1.12	8.73	10.05	0.06	0.34–0.68	13.03	26.11	0.3
1.12–1.68	7.2	7.11	−0.01	0.68–1.02	9.54	20.75	0.34
1.68–2.24	2.13	8.2	0.59	1.02–1.36	4.38	4.74	0.04
2.24–2.8	0.36	6.5	1.00	1.36–1.7	0.46	0.2	−0.38
Land-use Land-cover				Land-use Land-cover			
Bare Land	0.75	1.70	0.35	Bare Land	8.90	10.83	0.08
Built Area	18.98	18.97	−0.0002	Built Area	0.24	0.33	0.13
Clouds	0.0002	0	0	Clouds	0.0005	0	0
Crops	0.28	0	0	Crops	0.16	1.07	0.81
Rangeland	37.74	59.69	0.19	Rangeland	45.35	49.54	0.04
Snow/Ice	2.68	0	0	Snow/Ice	15.62	0.66	−1.37
Trees	39.35	18.73	−0.32	Trees	29.02	34.45	0.07
Water	0.21	0.90	0.62	Water	0.70	3.10	0.64
Rainfall				Rainfall			
96.73–101.88	10.21	16.83	0.21	61.19–71.43	41.30	29.62	−0.14
101.89–105.67	18.75	24.37	0.11	71.44–82.43	20.25	15.29	−0.12
105.68–109.21	26.97	26.22	−0.01	82.44–95.93	13.88	3.98	−0.54
109.22–112.43	25.45	20.19	−0.10	95.94–108.68	11.09	13.7	0.09
112.44–117.26	18.61	12.37	−0.17	108.69–124.92	13.46	37.40	0.44
Distance from Fault lines				Distance from Fault lines			
0–200	11.57	17.21	0.17	0–200	2.01	0.51	−0.59
200–400	10.94	13.94	0.10	200–400	2.01	2.63	0.11
400–600	10.14	9.00	−0.05	400–600	1.99	1.32	−0.17
600–800	9.23	8.25	−0.05	600–800	1.94	0.83	−0.37
>800	58.12	51.60	−0.05	>800	92.04	94.70	0.01

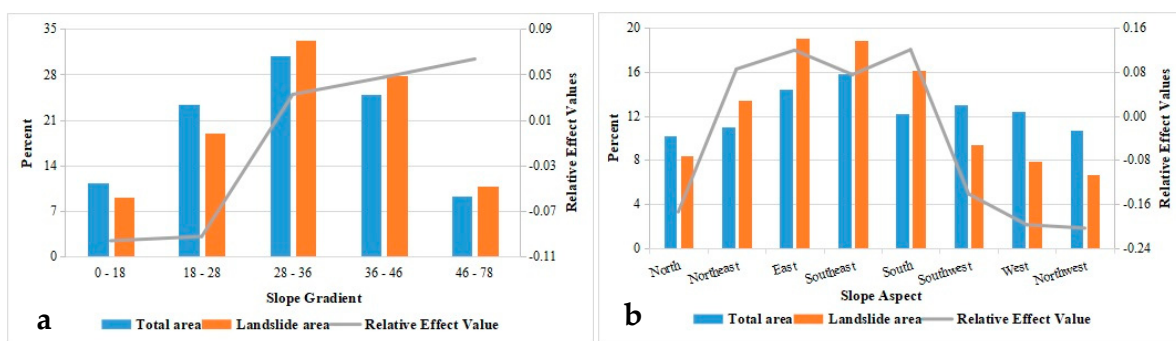


Figure 6. Cont.

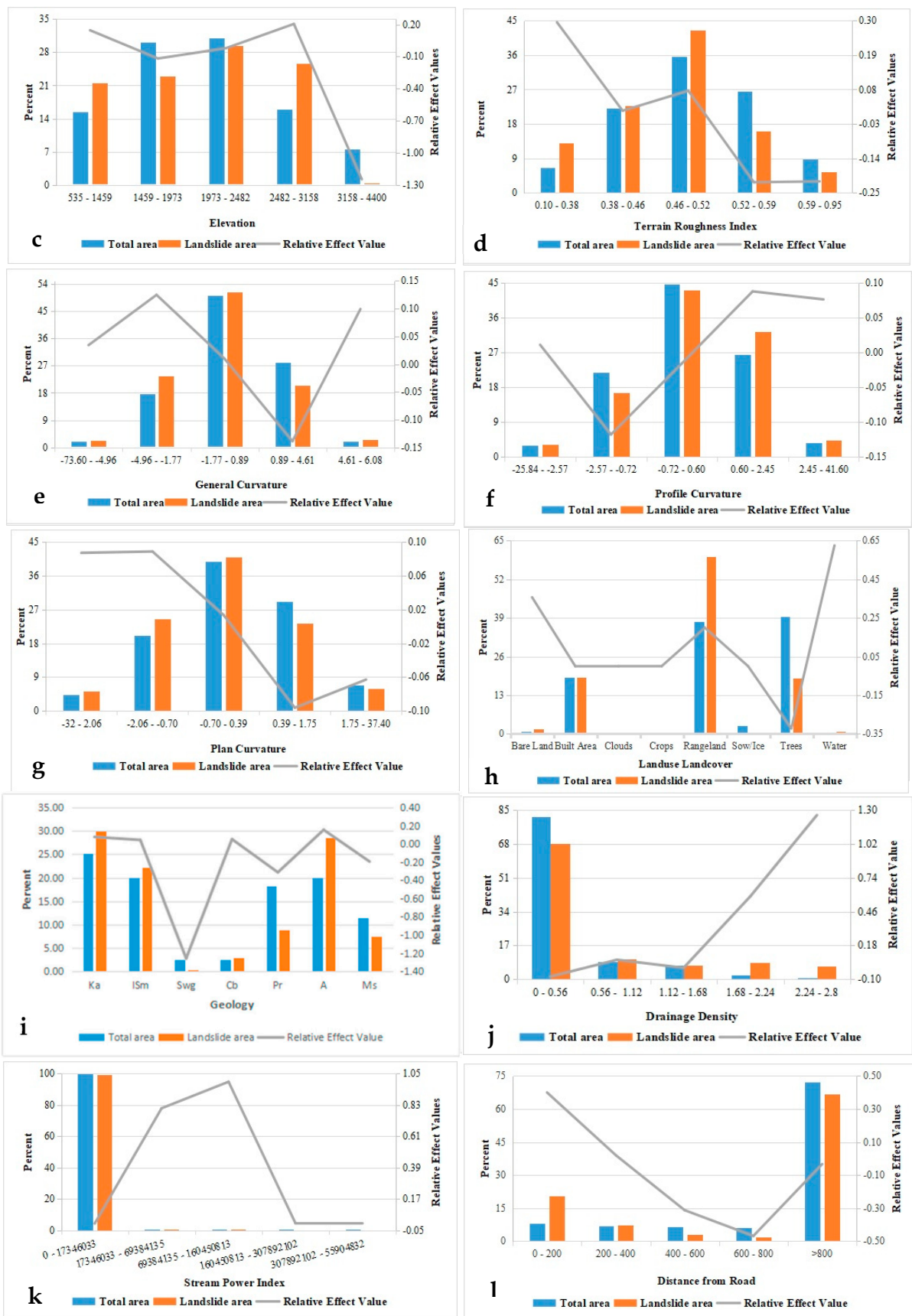


Figure 6. Cont.

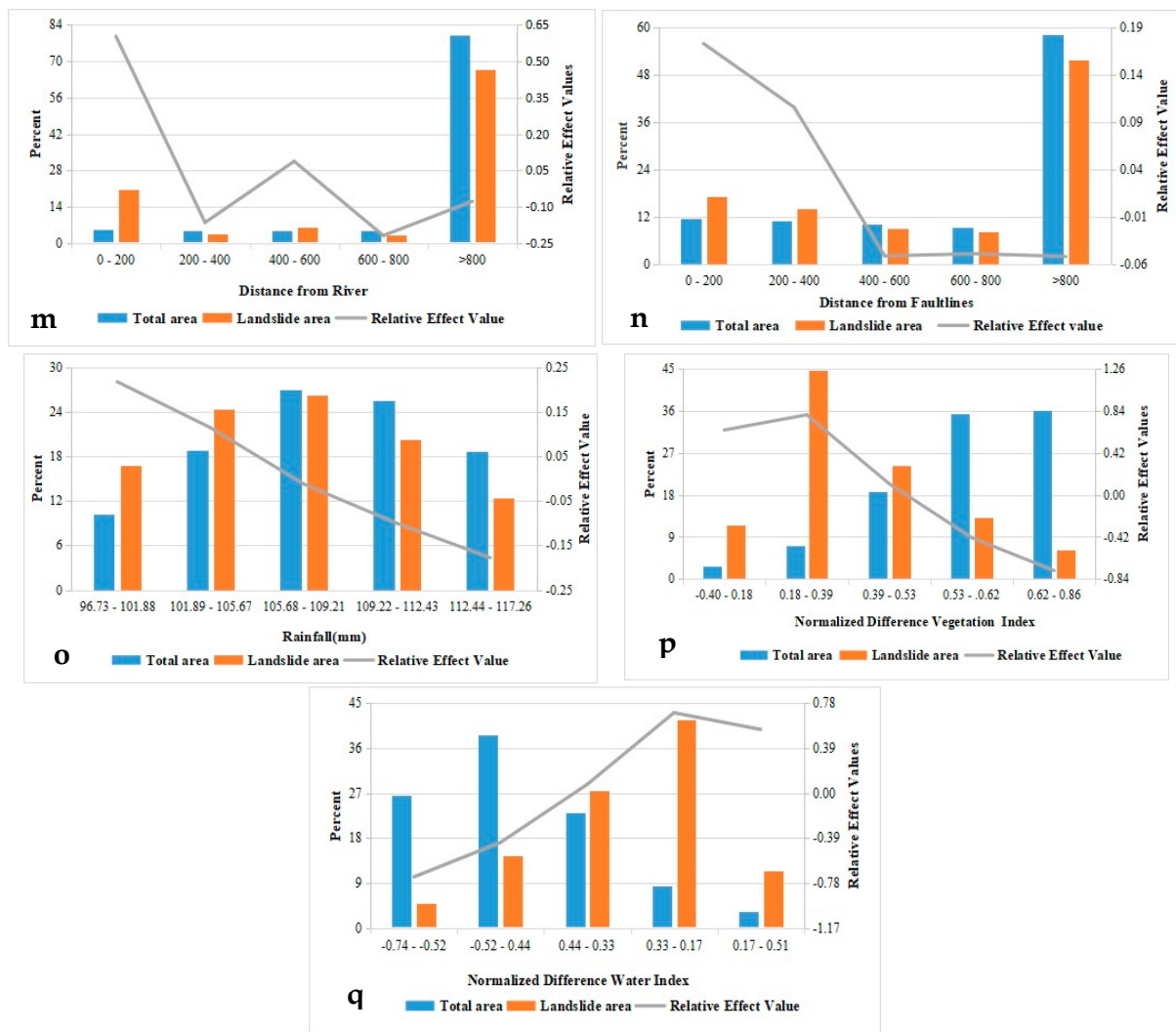


Figure 6. Relationship of landslides with the causative factors and relative effect values of the Alpuri Valley: (a) slope gradient; (b) slope aspect; (c) elevation; (d) terrain roughness index; (e) general curvature; (f) profile curvature; (g) plan curvature; (h) land-use land-cover; (i) geology; (j) drainage density; (k) stream power index; (l) distance to road; (m) distance to river; (n) distance from fault lines; (o) rainfall data; (p) NDVI; (q) NDWI.

4.3. Relationship of Landslides Occurrence with Causative Factors

In the Alpuri Valley, the resultant map of the slope gradient determines that slopes above 36 degree have a high concentration of landslide events, whereas in the Neelum Valley, the slopes above 38 degrees exhibit a high tendency for landslide events. The class with a slope gradient between 46–78 degrees showed highest relative effect value of 0.064 followed by the class 36–46 degrees (with RF of 0.047) in the Alpuri Valley, whereas the class with a slope gradient of 38–48 degrees represented highest relative effect value of 0.06 followed by the class 48–84 degrees (RF = 0.05) in the Neelum Valley. The gentle slope showed negative relative effect weights, and, hence, a lower possibility of landslide occurrence (Figures 6a and 7a, and Table 3).

Slope aspect factor, which depends on the duration of solar intensity and precipitation, describes the dimension of slopes. The highest relative effect value of slope aspect was found in the east and southward aspects, having a value of 0.12, and revealed high correlation with landslide occurrence in the Alpuri Valley. In the Neelum Valley, the highest relative effect value was observed in the north direction with a value of 0.31, showing a high impact on landslide events (Figures 6b and 7b, and Table 3).



Figure 7. Cont.

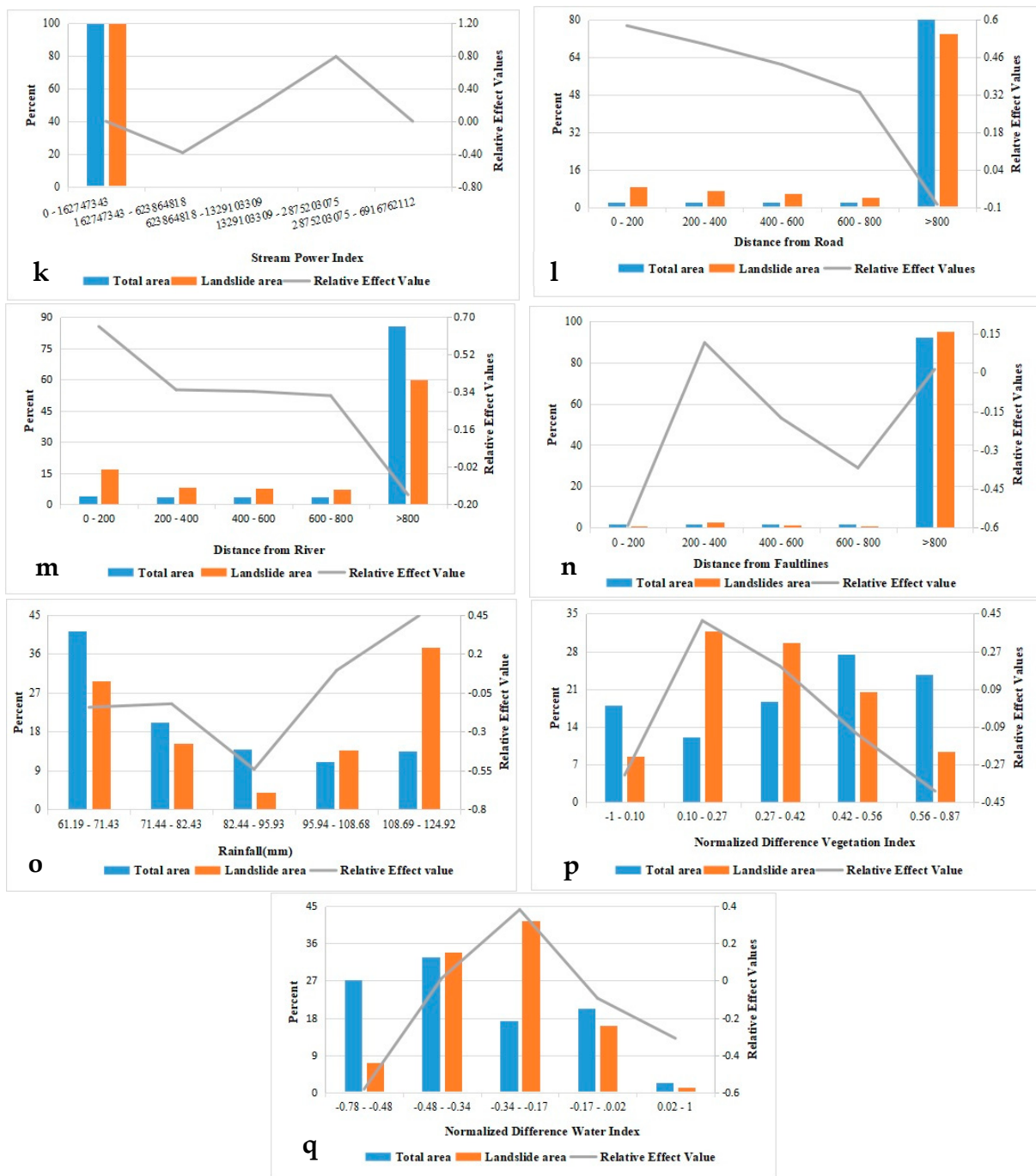


Figure 7. Relationship of landslides with the causative factors and relative effect values of the Neelum Valley: (a) slope gradient; (b) slope aspect; (c) elevation; (d) terrain roughness index; (e) general curvature; (f) profile curvature; (g) plan curvature; (h) land-use land-cover; (i) geology; (j) drainage density; (k) stream power index; (l) distance to road; (m) distance to river; (n) distance from fault lines; (o) rainfall data; (p) NDVI; (q) NDWI.

The elevation factor indicates that the class 2482–3158 m in the Alpuri Valley shows the highest relative affect value of 0.21, whereas, the in Neelum Valley, class 980–2219 m exhibits the highest relative effect value, equal to 0.46. These two classes of elevation reveal a high possibility of landslide occurrence in the study areas. The negative RE values have no influence on the landslide events (Figures 6c and 7c, and Table 3).

In the case of TRI factor, Table 3 and Figures 6d and 7d show that in the Alpuri Valley, the first (0.10–0.38) and third (0.46–0.52) classes, while in the Neelum Valley, the first

(0.08–0.38) and second (0.38–0.45) classes reveal that landslide events have a significant influence on these classes of TRI factor. It indicates that the erosion process is modifying the slope degree of the terrain.

General curvature contains three regions that are convex, concave, and flat. Every region has its impact and relation to landslide occurrence. In the Alpuri region, the concave region shows a high effect of landslide occurrence with a relative effect value of 0.12, observed in the class -4.96 to -1.77 . The convex region also represents a high landslide influence in the class 4.61 to 6.08 with a relative effect value of 0.1. In the Neelum Valley, concave landforms show a high relative effect value in the class -54.64 to -4.48 ($RE = 0.25$) followed by the class -4.48 to -1.28 ($RE = 0.11$), and exhibit a high impact of landslide hazard (Table 3, Figures 6e and 7e).

In the case of profile curvature for the Alpuri region, the concave region has a high relative effect value, representing a high concentration of landslide occurrence, especially in class 2.45 – 41.60 and 0.60 – 2.45 with relative effect values of 0.08 and 0.09, respectively (Table 3, Figures 6f and 7f). For the Neelum Valley, the concave region in the class 2.7 – 38.12 has a relative effect value of 0.25, representing a high relative effect value. The flat region demonstrated no effect of landslide. The comparative analysis of the valleys indicates that the concave landforms have a high probability of landslide occurrence compared to the convex and flat landforms.

In case of plan curvature, the concave region exhibits a high relative effect of 0.09 in the class -32 to -2.06 and the class -2.06 to -0.7 , with a high volume in these curvature classes of the Alpuri area. In the Neelum Valley, the concave region also reveals high relative effect values of 0.23 and 0.15 in the class -38.9 to -2.83 and the class -2.83 to 1.04 , respectively. These concave regions have a high concentration of landslide events as compared to the flat and convex regions of the study areas (Table 3, Figures 6g and 7g).

The land-use land-cover (LULC) factor also plays an important role in slope instability. The study regions' likelihood of experiencing landslides is indicated by eight distinct classes with varying landslide concentrations and relative effect values. Positive relative effect values were observed in the LULC classes of bare land, rangeland, and water of the Alpuri region, while in the Neelum region, LULC classes such as bare land, built area, crops, rangeland, and water exhibited positive relative effect values, indicating a strong correlation with landslide occurrence (Table 3, Figures 6h and 7h).

The lithological units in the Alpuri region such as Kamila amphibolite complex (Ka), Archean (A), Cambrian Manglaur (Cb), and Indus suture mélange (Ism), and the lithological units in the Neelum Valley, for instance, Mansehra granite (Mg) and Salkhala group (Pr), exhibit positive relative effect values (Table 3, Figures 6i and 7i). These units are brittle and immature with sand and silt in the soil that contribute tremendously towards landslide occurrences.

In general, an increase in landslide events with a decrease in the distance to the streams indicates a direct relationship between the occurrences of landslides in the vicinity of streams. According to relative effect values of drainage density, the fifth class (2.24 to 2.8) determined a high influence of landslide occurrence in the Alpuri Valley, while the third class (0.68 to 1.02) identified the high influence of landslide events in the Neelum region. Table 3 and Figures 6j and 7j show an overall correlation between drainage density, landslide occurrences, and relative effect value.

Stream power index (SPI) is used to determine the erosion power of water. Comparing the results of both valleys, the third class of SPI in the Alpuri region shows a high relative effect value of 0.99, whereas the fourth class of SPI reveals a high relative effect value of 0.8 in the Neelum Valley. These values represent a high probability of landslide events in areas with these classes, owing to the high probability of erosion power (Table 3, Figures 6k and 7k).

The tendency of landslide events is observed to be high near the roads, and tendency is gradually decreased away from the roads. The class with 0 – 200 m has the highest relative effect values of 0.4 in the Alpuri Valley, and 0.58 in the Neelum Valley (Table 3, Figures 6l and 7l), indicating more chances of landslide events near the roads.

The Alpuri Valley and the Neelum Valley exhibit similar results for 0–200 m distance class from rivers. It shows a high probability of landslide occurrence near the rivers. For this distance to road class, a highest value of 0.60 was observed in the Alpuri region, while 0.65 was observed in the Neelum Valley (Table 3, Figures 6m and 7m).

The distance to fault line class of 0 and 400 m in the Alpuri region exhibits a high concentration of landslides and, hence, exhibits high relative effect values, indicating a zone highly affected by landslides. However, their effectiveness is decreased for locations more distant from the fault line. The class 400 to >800 m represented a low concentration of landslides due to negative relative effect values. In case of the Neelum Valley, the distance to fault line class of 200–400 m and class >800 m indicates high relative effect values with a high concentration of landslides representing a high correlation with landslide occurrence (Table 3, Figures 6n and 7n). This behavior reveals that distance from fault line is less effective for landslide occurrences in the Neelum Valley as compared to other responsible factors.

Rainfall is one of the triggering factors to enhance slope instability. According to the rainfall data, the Alpuri Valley's low rainfall area (96.73 to 105.67 mm) constituted an area with a high occurrence of landslides. On the other hand, the high rainfall area showed a negative relative effect value, indicating that it was less affected by landslides. The relative effect curve showed a gradual decrease from low to high concentrations of rainfall. High rainfall regions in the Neelum Valley, with rainfall ranging from 95.95 to 124.92 mm, exhibited higher relative effect values as compared to other classes (Table 3, Figures 6o and 7o).

NDVI represents the difference between green vegetation and the non-vegetation area. According to the results of the NDVI factor, landslides are less common in areas with high concentrations of vegetation (NDVI = 0.56–0.87), whereas landslides are more common in areas with low concentrations of vegetation (NDVI = 0.10–0.27). In the instance of the Alpuri region, the relative effect model indicates that NDVI class of 0.18–0.39 demonstrates a high concentration of landslide occurrences owing to a low concentration of vegetation, whereas NDVI class of 0.62–0.86 shows no influence of landslide due to a high concentration of vegetation (Table 3, Figures 6p and 7p).

NDWI factor represents the presence of water bodies in the respective study areas. In the Alpuri Valley, the NDWI class of 0.33–0.17, with a relative effect value of 0.7, was found to be highly prone to landslides, while the NDWI class -0.74 to -0.52 has a low relative effect value equivalent to -0.73 , indicating a low concentration of landslides. For the Neelum valley, the NDWI class of -0.34 to -0.17 indicates a high landslide occurrence (Table 3, Figures 6q and 7q).

4.4. Landslide Susceptibility Mapping and Zonation

Landslides affect the natural and socioeconomic environments in the Neelum and Alpuri Valleys. Landslide susceptibility zonation is an appropriate way for better planning and mitigation in landslide-prone areas. Based on the contributing factors, landslide-prone zones are categorized into low, moderate, high, and extremely high zones. The GIS environment was used to overlay all of these themes in order to create the study area's landslide zonation map. The relative effect model, which is a quantitative approach, is utilized to assess the significance of each class in each factor map. Using the landslide susceptibility index (Equation (9)), all themes were summed up to create the landslide susceptibility zonation map.

In the Neelum Valley, the landslide susceptibility index was in the range from -8.37 to 5.88 in the Neelum region, whereas in the Alpuri Valley, it ranged between -5.30 and 5.65 . The landslide susceptibility index maps were categorized into four zones (Figure 8), namely, very high, high, moderate, and low. The percent area of extremely high class in the Alpuri and Neelum regions were observed to be 7.55% and 18.14%, respectively (Table 4 and Figure 9). Parts of the study areas in proximity to the roads and rivers have higher percentages of high class, which are 25.33% (Alpuri) and 34.04% (Neelum). The entire high landslide susceptibility zones were found to be 52.18% in the Neelum Valley and 32.88% in the Alpuri Valley. Comparing the

results from both study sites, the Neelum Valley (the Himalaya) was found to be more prone to landslide hazards than the Alpuri Valley (the Hindukush).

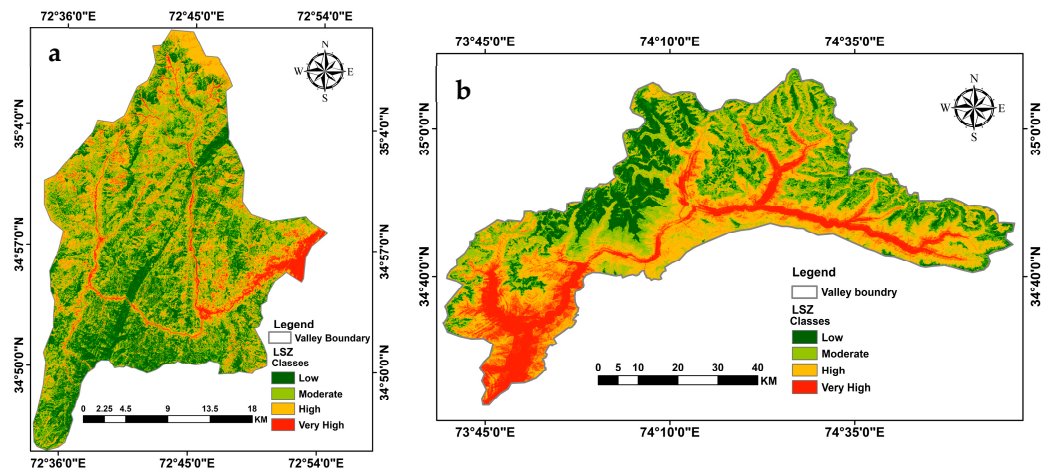


Figure 8. Landslide susceptibility maps (a) Alpuri Valley and (b) Neelum Valley.

Table 4. Landslide susceptibility zone of Alpuri Valley.

Zones	Low	Moderate	High	Very High
Alpuri Valley	27.31	39.81	25.33	7.55
Neelum Valley	17.56	30.26	34.04	18.14

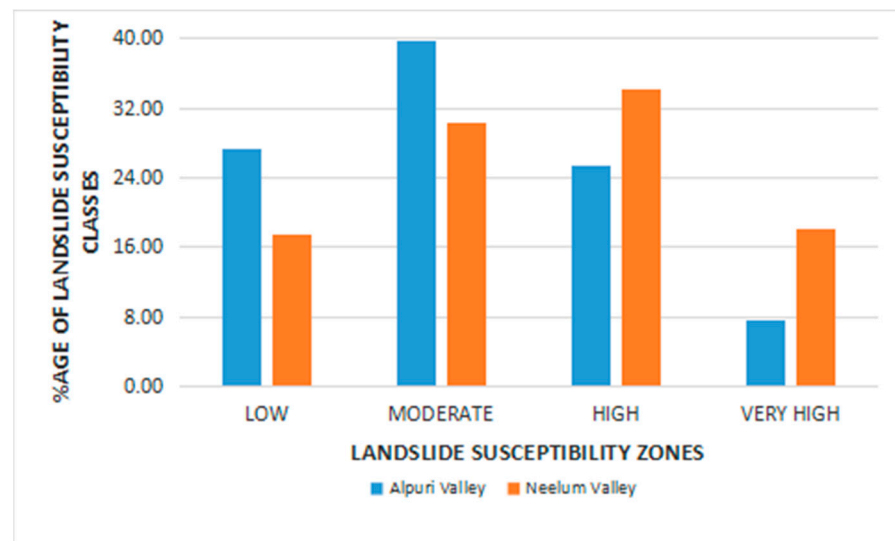


Figure 9. Landslide susceptibility zones of Alpuri Valley and Neelum Valley.

4.5. Model Validation

In order to develop and validate the landslide susceptibility map, the landslides inventory was divided into two sets, comprising a 70% training dataset and a 30% validation dataset. A total of 70% of the landslide inventory was used for the modelling, and 30% of the landslide inventory was used for the validation of the model results. The accuracy and performance of the landslide susceptibility maps developed by relative effect (RE) model were verified by receiver operating characteristics (ROC). Area under the ROC curve (AUC) was used to evaluate the capacity of the model to predict the occurrence and non-occurrence of landslide events. The success rate curve was prepared using the 70% landslide inventory with landslide susceptibility maps. The prediction rate curve was prepared using 30% of the remaining landslide inventory with landslide susceptibility

maps to check the performance and validation of the model in the study regions. Above the value of 80% of the AUC, the index exhibited an excellent classification model [50].

In this study, the model comparison and validation using the 70% training data and 30% testing data were carried out in study areas with different spatial coverage. A total of 17 similar causative factors were used in the Alpuri Valley and the Neelum Valley to prepare the landslide susceptibility maps, and evaluate the ability of relative effect model in these valleys. Figure 10 shows a success rate curve of 74.75% and 82.15% for the Alpuri Valley and the Neelum Valley, respectively. The prediction accuracy in the Alpuri and Neelum Valleys was calculated at 87.87% and 82.73%, respectively. Plausible results for the Neelum Valley are indicated by the success rate curve and AUC value. However, the prediction rate curve and AUC value show that the relative effect model has excellent accuracy in the Alpuri Valley, once the model's appropriateness and validation are evaluated. As a result, it is suggested that the model employed here, for mapping the susceptibility of landslides, is suitable for both local and regional scales.

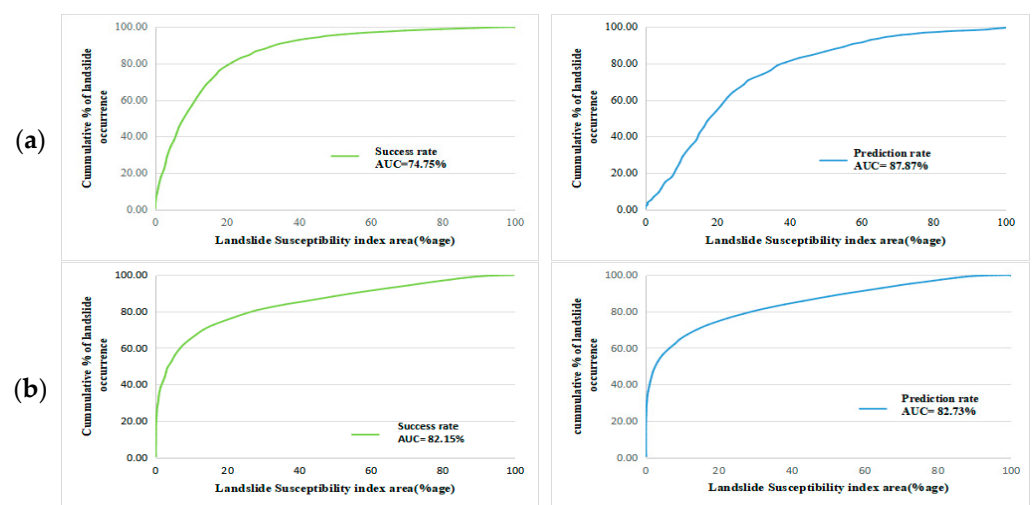


Figure 10. Success and prediction curves of (a) Alpuri Valley (b) Neelum Valley.

5. Discussion

Landslide susceptibility assessment is an important tool that gives valuable information for the areas that are affected by slope failure. Several approaches to landslide susceptibility have been studied and suggested by various researchers to study landslides-prone areas [51–53]. In this study, the relative effect model was used to assess landslide susceptibility by evaluating the relationship of various causative factors with landslides. In most of the approaches, the landslide susceptibility mapping process is similar where landslide causative parameters and landslide inventory maps are incorporated to categorize the study area into different susceptibility zones [54–56]. Selection of suitable and critical causative factors is imperative for the accuracy of landslide susceptibility [18,57]. Nevertheless, selection of causative factors can vary and is highly dependent on the topographic and hydro-meteorological characteristics of the study area. There is no universal standard for the selection of causative factors.

This study prepared a detailed landslide inventory that divided it into three types of landslides, such as slide, debris flow, and rock fall. These types were observed at the time of the field survey. The number of slides is higher in both study areas than debris flow and rock fall. With respect to area coverage, debris flow has covered a larger area than slides and rock falls. Debris flow is caused by heavy rainfall during the rainy seasons. The debris flow travels long distances due to high elevation and steep surfaces.

The landslides inventory and integration of specific landslide causative elements constitute the model database. The weightage result of influencing factors that have a high likelihood and a high relative effect value determines the probability of a landslide

occurrence. The relative effect model is able to identify the different components that cause/trigger landslides in an objective manner. These various causative factors are integrated into the GIS environment to generate the final susceptibility map.

In this study, among the causative factors, the relative effect model is applied to observe the significance of various causative factors. Plan curvature, rainfall, profile curvature, distance from fault lines, distance from streams, LULC, slope aspect, drainage density, stream power index, NDVI, and NDWI contribute to landslide occurrences in the Alpuri Valley, while in the Neelum Valley, terrain roughness index, drainage density, plan curvature, profile curvature, general curvature, geology, land-use land-cover, stream power index, and distance from streams and roads have a significant influence on the spatial distribution of landslides.

The most susceptible geological/lithological units to landslides are the Besham group and the Kamila amphibolite complex in the Alpuri Valley, whereas Surgun group A, Mansehra granites, and the Salkhala group are more susceptible to landslides in the Neelum Valley. Spatial coverage of the Besham group and Kamila amphibolite complex is 28.59% and 30.01%, respectively, in the Alpuri region. The spatial coverage of Surgun group A, Mansehra granites, and the Salkhala group are 6.34%, 20.29%, and 31.69%, respectively, in the Neelum Valley.

With respect to slope gradient, in both study regions, slope gradient >29 degrees indicated a positive relationship with landslide occurrences. The spatial coverage of slope gradient >29 is 71.98% in the Alpuri region, whereas it is 69.13% in the Neelum Valley. The results of slope gradient of both valleys demonstrate that an increase in the slope gradient results in an increase in the landslide ratio.

The northeast and south aspects of the Alpuri Valley and the northeast and south aspects of the Neelum Valley are more susceptible to landslides and exhibit a positive correlation with landslide occurrences.

Elevation factor shows that elevation between 2482–3158 m has a high correlation with the landslide events in the Alpuri Valley, while the elevation class of 980–2887 m is more susceptible to landslide occurrence in the Neelum Valley.

Regarding the terrain roughness index, the most susceptible index was 0.10 to 0.52 in the Alpuri Valley compared to 0.08 to 0.45 in Neelum valley. These indices indicate the erosion process with respect to a change in the terrain slope.

General curvature determines the impact of flat, concave, and convex curves on terrain slope leading to landslide. Slopes with concave curvature are more susceptible to landslides in the Alpuri Valley and the Neelum Valley. For plan curvature, the same results were found in the Alpuri and Neelum Valleys, where concave curvature showed a positive correlation with landslide events and, hence, meant they were more susceptible to landslide occurrence.

Among LULC classes, bare land, water bodies, and rangeland showed a positive correlation with landslides occurrence due to no cohesive forces in soil particles, low infiltration rate, and no vegetation.

The stream power index (SPI) shows the erosion power of water. The high flow of water indicates that a high erosion process in the streams leads to landslides along the riversides. In the Alpuri Valley, the second and third classes of SPI were found to be more susceptible to landslide occurrence, while the third and fourth SPI classes exhibited a high probability of landslides with positive correlation in the Neelum Valley.

The impact of moisture content on the material present on the slopes, toe-cutting process and drainage density favors landslides and reduces the slope stability. The result of drainage density shows that the high drainage density class of 1.68–2.8 in the Alpuri Valley and the 0.34 to 1.36 drainage density class in the Neelum Valley are more susceptible to landslide occurrence.

In the case of distance from roads and rivers, 200 m in the Alpuri Valley and 800 m in the Neelum Valley show a positive correlation with landslide events. Both study areas are seismically and tectonically active. In the Alpuri Valley, the distance from fault line

ranging from 0 to 400 m shows the highest landslide concentration, whereas the 200–400 m class exhibits a high probability of landslide. Class 0–400 m (distance from roads) exhibits a high probability of landslides due to high RE values in the Alpuri Valley. Distance to roads ranging from 200 to 400 m shows a high correlation with landslide occurrence in the Neelum Valley.

Intensive rainfall is the major triggering force for landslides in the study areas. During the rainy season, old landslides are reactivated along with new landslides. It was observed that 96.73 mm to 105.67 mean monthly rainfall indicated a positive correlation with landslide occurrences in the Alpuri Valley. Mean monthly rainfall ranging from 108.69 to 124.92 mm showed a high probability of landslides in the Neelum Valley.

With respect to NDVI, the no-vegetation classes in the study area were observed to be more susceptible classes and, hence, showed the highest RE values. The vegetation cover class is least prone to landslide. Among the NDWI, the class ranging from 0.17 to 0.51 reveals the presence of a water body and, hence, a positive correlation with landslide occurrence in the Alpuri Valley, while the NDWI class ranging from -0.34 to 0.17 is found to be more susceptible to landslide occurrence in the Neelum Valley.

Accuracy and validity of the susceptibility maps of study areas shows that RE model results are proven to be more accurate in the Alpuri Valley than in the Neelum Valley. The success rate curves in the Alpuri Valley are 74.75%, while those in the Neelum Valley are 81.15%. The prediction power of the RE model was determined using the prediction rate curve. In the Alpuri and Neelum Valleys, the prediction accuracy for the RE model is 87.87% and 82.73%, respectively.

6. Conclusions

A relative effect model, a bivariate model, was used for conducting a landslide susceptibility assessment in two mountainous regions located in Hindukush (Alpuri Valley) and Himalaya (Neelum Valley), being landslide-prone areas in northern Pakistan. The main objective of this research was to evaluate the suitability, accuracy, and performance of the relative effect model for landslide susceptibility mapping. The Alpuri Valley is three times smaller than the Neelum Valley in size. The initial step was to identify and map past landslides using GIS software. There have been 89 and 368 landslides in the Alpuri Valley and Neelum Valley, respectively, in the past. These landslides included slides, debris flow, and rock fall. Among the mapped landslides, slides are the most dominant type of landslides in both study areas. A total of 17 causative factors were developed and correlated with landslide inventory through the relative effect model for the preparation of a landslide susceptibility map to determine landslide-vulnerable regions for the future, using remotely sensed and departmental data in GIS. The final map of the study areas shows four landslide susceptibility classes, including low, moderate, high, and very high. Regarding the model validation, the success curve result of the study areas indicated 74.75% in the Alpuri Valley and 82.15% in the Neelum Valley, while the prediction curve showed 87.87% in the Alpuri Valley and 82.73% in the Neelum Valley. Prior to this research, different techniques were employed to compare the performance of different techniques in a single region; however, no comparison of a single technique was provided with two regions with differences in terms of size of the valley. This paper considered two study areas with the same causative factors and identified the performance and suitability of the method employed. This novel idea made a new step to evaluate the applicability of an existing technique and created interest for relevant researchers worldwide. From the comparison of model results, it has been concluded that the applicability, suitability, and performance of the RE model better suits a small area for landslide susceptibility mapping. The outcomes of this study from these two valleys can be applied for landslide hazard and risk assessment and further research in the study areas. Furthermore, it will support landslide mitigation plans and landslide hazard risk assessment in other areas vulnerable to landslides.

Author Contributions: Conceptualization, S.M.K. and A.-U.R.; Methodology, S.M.K., A.-U.R. and M.A.; Software, S.M.K., F.A., M.S. and S.U.; Validation, M.S. and S.U.; Formal analysis, M.A.; Investigation, S.U.; Data curation, A.-U.R. and F.A.; Writing—original draft, S.M.K.; Writing—review & editing, M.A. and M.S.; Visualization, M.S.; Supervision, A.-U.R. and M.A.; Project administration, F.A.; Funding acquisition, F.A. All authors have read and agreed to the published version of the manuscript.

Funding: This research was funded by Abdullah Alrushaid Chair for Earth Science Remote Sensing Research at King Saud university, Riyadh, Saudi Arabia.

Institutional Review Board Statement: Not applicable.

Informed Consent Statement: Not applicable.

Data Availability Statement: All the data published in this article will be available on request to the corresponding authors.

Acknowledgments: The authors extend their appreciation to Abdullah Alrushaid Chair for Earth Science Remote Sensing Research at King Saud university for funding.

Conflicts of Interest: The authors declare no conflicts of interest.

References

- Dou, J.; Yunus, A.P.; Bui, D.T.; Merghadi, A.; Sahana, M.; Zhu, Z.; Chen, C.-W.; Han, Z.; Pham, B.T. Improved landslide assessment using support vector machine with bagging, boosting, and stacking ensemble machine learning framework in a mountainous watershed, Japan. *Landslides* **2020**, *17*, 641–658. [\[CrossRef\]](#)
- Dagdelenler, G.; Nefeslioglu, H.A.; Gokceoglu, C. Modification of seed cell sampling strategy for landslide susceptibility mapping: An application from the Eastern part of the Gallipoli Peninsula (Canakkale, Turkey). *Bull. Eng. Geol. Environ.* **2016**, *75*, 575–590. [\[CrossRef\]](#)
- Kirschbaum, D.; Stanley, T.; Zhou, Y. Spatial and temporal analysis of a global landslide catalogue. *Geomorphology* **2015**, *249*, 4–15. [\[CrossRef\]](#)
- Froude, M.J.; Petley, D.N. Global fatal landslide occurrence from 2004 to 2016. *Nat. Hazards Earth Syst. Sci.* **2018**, *18*, 2161–2181. [\[CrossRef\]](#)
- Alshehri, F.; Sultan, M.; Karki, S.; Alwagdani, E.; Alsefry, S.; Alharbi, H.; Sahour, H.; Sturchio, N. Mapping the Distribution of Shallow Groundwater Occurrences Using Remote Sensing-Based Statistical Modeling over Southwest Saudi Arabia. *Remote Sens.* **2020**, *12*, 1361. [\[CrossRef\]](#)
- Owen, L.A.; Kamp, U.; Khattak, G.A.; Harp, E.L.; Keefer, D.K.; Bauer, M.A. Landslides triggered by the 8 October 2005 Kashmir earthquake. *Geomorphology* **2008**, *94*, 1–9. [\[CrossRef\]](#)
- Weissel, J.K.; Stark, C.P. Landslides triggered by the 1999 Mw7. 6 Chi-Chi earthquake in Taiwan and their relationship to topography. In *Scanning the Present and Resolving the Future, Proceedings of the IAGRS 2001, IEEE 2001 International Geoscience and Remote Sensing Symposium (Cat. No. 01CH37217), Sydney, NSW, Australia, 9–13 July 2001*; IEEE: Piscataway, NJ, USA, 2001; Volume 2, pp. 759–761.
- Xu, C. Preparation of earthquake-triggered landslide inventory maps using remote sensing and GIS technologies: Principles and case studies. *Geosci. Front.* **2015**, *6*, 825–836. [\[CrossRef\]](#)
- Kamp, U.; Growley, B.J.; Khattak, G.A.; Owen, L.A. GIS-based landslide susceptibility mapping for the 2005 Kashmir earthquake region. *Geomorphology* **2008**, *101*, 631–642. [\[CrossRef\]](#)
- Shano, L.; Raghuvanshi, T.K.; Meten, M. Landslide susceptibility evaluation and hazard zonation techniques—A review. *Geoenviron. Disasters* **2020**, *7*, 18. [\[CrossRef\]](#)
- Reichenbach, P.; Rossi, M.; Malamud, B.D.; Mihir, M.; Guzzetti, F. A review of statistically-based landslide susceptibility models. *Earth-Sci. Rev.* **2018**, *180*, 60–91. [\[CrossRef\]](#)
- Akgun, A.; Erkan, O. Landslide susceptibility mapping by geographical information system-based multivariate statistical and deterministic models: In an artificial reservoir area at Northern Turkey. *Arab. J. Geosci.* **2016**, *9*, 165. [\[CrossRef\]](#)
- Ahmad, K.S.; Hameed, M.; Fatima, S.; Ashraf, M.; Ahmad, F.; Naseer, M.; Zahoor, A.; Ahmad, I. Tribe Andropogoneae from Neelum Valley, Azad Jammu and Kashmir: Phylogeny Based On Morpho-Anatomy. *Pak. J. Bot.* **2017**, *49*, 73–82.
- Rahman, A.-U.; Khan, A.N.; Collins, A.E. Analysis of landslide causes and associated damages in the Kashmir Himalayas of Pakistan. *Nat. Hazards* **2014**, *71*, 803–821. [\[CrossRef\]](#)
- Van Den Eeckhaut, M.; Reichenbach, P.; Guzzetti, F.; Rossi, M.; Poesen, J. Combined landslide inventory and susceptibility assessment based on different mapping units: An example from the Flemish Ardennes, Belgium. *Nat. Hazards Earth Syst. Sci.* **2009**, *9*, 507–521. [\[CrossRef\]](#)
- Park, S.; Choi, C.; Kim, B.; Kim, J. Landslide susceptibility mapping using frequency ratio, analytic hierarchy process, logistic regression, and artificial neural network methods at the Inje area, Korea. *Environ. Earth Sci.* **2013**, *68*, 1443–1464. [\[CrossRef\]](#)
- Guillard, C.; Zezere, J. Landslide susceptibility assessment and validation in the framework of municipal planning in Portugal: The case of Loures municipality. *Environ. Manag.* **2012**, *50*, 721–735. [\[CrossRef\]](#)

18. Yalcin, A.; Reis, S.; Aydinoglu, A.C.; Yomralioglu, T. A GIS-based comparative study of frequency ratio, analytical hierarchy process, bivariate statistics and logistics regression methods for landslide susceptibility mapping in Trabzon, NE Turkey. *Catena* **2011**, *85*, 274–287. [[CrossRef](#)]
19. Mika. Weathering of Igneous Rocks. 2013. Available online: <http://www.geomika.com/blog/2013/08/17/weathering-igneous/> (accessed on 1 September 2003).
20. Youssef, A.M.; Al-Kathery, M.; Pradhan, B. Landslide susceptibility mapping at Al-Hasher area, Jizan (Saudi Arabia) using GIS-based frequency ratio and index of entropy models. *Geosci. J.* **2015**, *19*, 113–134. [[CrossRef](#)]
21. Singh, S. *Geomorphology*; Prayag Pustak Bhawan: Allahabad, India, 2007.
22. Jebur, M.N.; Pradhan, B.; Tehrany, M.S. Manifestation of LiDAR-derived parameters in the spatial prediction of landslides using novel ensemble evidential belief functions and support vector machine models in GIS. *IEEE J. Sel. Top. Appl. Earth Obs. Remote Sens.* **2014**, *8*, 674–690. [[CrossRef](#)]
23. Riley, S.J.; DeGloria, S.D.; Elliot, R. Index that quantifies topographic heterogeneity. *Intermt. J. Sci.* **1999**, *5*, 23–27.
24. Bui, D.T.; Ho, T.C.; Revhaug, I.; Pradhan, B.; Nguyen, D.B. Landslide susceptibility mapping along the national road 32 of Vietnam using GIS-based J48 decision tree classifier and its ensembles. In *Cartography from Pole to Pole*; Springer: Berlin/Heidelberg, Germany, 2014; pp. 303–317.
25. Wang, Q.; Li, W.; Wu, Y.; Pei, Y.; Xing, M.; Yang, D. A comparative study on the landslide susceptibility mapping using evidential belief function and weights of evidence models. *J. Earth Syst. Sci.* **2016**, *125*, 645–662. [[CrossRef](#)]
26. Thomas, G.B. *Calculus and Analytic Geometry*; Addison-Wesley: Boston, MA, USA, 1968.
27. Ayalew, L.; Yamagishi, H. The application of GIS-based logistic regression for landslide susceptibility mapping in the Kakuda-Yahiko Mountains, Central Japan. *Geomorphology* **2005**, *65*, 15–31. [[CrossRef](#)]
28. Varnes, D.J. *Landslide Hazard Zonation: A Review of Principles and Practice*; United Nations: New York, NY, USA, 1984.
29. Hack, J.T.; Goodlett, J.C. *Geomorphology and Forest Ecology of a Mountain Region in the Central Appalachians*; United States Government Printing Office: Washington, DC, USA, 1960.
30. Dietrich, W.E. The importance of hollows in debris flow studies; Examples from Marin County, California. In *Debris Flows/Avalanches: Process, Recognition, and Mitigation*; Geological Society of America: Boulder, CO, USA, 1987; Volume 7, p. 165.
31. Carson, M.A.; Kirkby, M.J. (Eds.) *Hillslope Form and Process*; Cambridge University Press: London, UK, 1972; p. 475.
32. Kouli, M.; Loupasakis, C.; Soupios, P.; Vallianatos, F. Landslide hazard zonation in high-risk areas of Rethymno Prefecture, Crete Island, Greece. *Nat. Hazards* **2010**, *52*, 599–621. [[CrossRef](#)]
33. Ayalew, L.; Yamagishi, H. Slope failures in the Blue Nile basin, as seen from landscape evolution perspective. *Geomorphology* **2004**, *57*, 95–116. [[CrossRef](#)]
34. Montgomery, D.R.; Schmidt, K.M.; Greenberg, H.M.; Dietrich, W.E. Forest clearing and regional landsliding. *Geology* **2000**, *28*, 311–314. [[CrossRef](#)]
35. Alshehri, F.; Abd El-Hamid, H.T.; Mohamed, A. Mapping coastal groundwater potential zones using remote sensing based AHP model in Al Qunfudhah region along Red Sea, Saudi Arabia. *Heliyon* **2024**, *10*, e28186. [[CrossRef](#)] [[PubMed](#)] [[PubMed Central](#)]
36. Strahler, A.N. Quantitative Geomorphology of Drainage Basins and Channel networks. In *Handbook of Applied Hydrology*; Chow, V.T., Ed.; McGraw-Hill: New York, NY, USA, 1964; pp. 411–476.
37. Moore, I.D.; Wilson, J.P. Length-slope factors for the Revised Universal Soil Loss Equation: Simplified method of estimation. *J. Soil Water Conserv.* **1992**, *47*, 423–428.
38. Oh, H.-J.; Pradhan, B. Application of a neuro-fuzzy model to landslide-susceptibility mapping for shallow landslides in a tropical hilly area. *Comput. Geosci.* **2011**, *37*, 1264–1276. [[CrossRef](#)]
39. Jaafari, A.; Najafi, A.; Pourghasemi, H.R.; Rezaeian, J.; Sattarian, A. GIS-based frequency ratio and index of entropy models for landslide susceptibility assessment in the Caspian forest, northern Iran. *Int. J. Environ. Sci. Technol.* **2014**, *11*, 909–926. [[CrossRef](#)]
40. Zhao, C.; Chen, W.; Wang, Q.; Wu, Y.; Yang, B. A comparative study of the statistical index and certainty factor models in landslide susceptibility mapping: A case study for the Shangzhou District, Shaanxi Province, China. *Arab. J. Geosci.* **2015**, *8*, 9079–9088. [[CrossRef](#)]
41. Mancini, F.; Ceppi, C.; Ritrovato, G. GIS and statistical analysis for landslide susceptibility mapping in the Daunia area, Italy. *Nat. Hazards Earth Syst. Sci.* **2010**, *10*, 1851–1864. [[CrossRef](#)]
42. Sujatha, E.R.; Rajamanickam, G.V.; Kumaravel, P. Landslide susceptibility analysis using Probabilistic Certainty Factor Approach: A case study on Tevankarai stream watershed, India. *J. Earth Syst. Sci.* **2012**, *121*, 1337–1350. [[CrossRef](#)]
43. Swanson, F.J.; Dyrness, C.T. Impact of clear-cutting and road construction on soil erosion by landslides in the western Cascade Range, Oregon. *Geology* **1975**, *3*, 393–396. [[CrossRef](#)]
44. Larsen, I.J.; Montgomery, D.R. Landslide erosion coupled to tectonics and river incision. *Nat. Geosci.* **2012**, *5*, 468–473. [[CrossRef](#)]
45. Chen, W.; Li, W.; Chai, H.; Hou, E.; Li, X.; Ding, X. GIS-based landslide susceptibility mapping using analytical hierarchy process (AHP) and certainty factor (CF) models for the Baozhong region of Baoji City, China. *Environ. Earth Sci.* **2016**, *75*, 63. [[CrossRef](#)]
46. Tibaldi, A.; Ferrari, L.; Pasquarè, G. Landslides triggered by earthquakes and their relations with faults and mountain slope geometry: An example from Ecuador. *Geomorphology* **1995**, *11*, 215–226. [[CrossRef](#)]
47. Felicísimo, Á.M.; Bonham-Carter, G.F. (1996): Geographic information systems for geoscientists. Modelling with GIS. *GeoFocus Rev. Int. Cienc. Tecnol. Inf. Geográfica* **2003**, *20*, 9–12.

48. Du, G.-L.; Zhang, Y.-S.; Iqbal, J.; Yang, Z.-H.; Yao, X. Landslide susceptibility mapping using an integrated model of information value method and logistic regression in the Bailongjiang watershed, Gansu Province, China. *J. Mt. Sci.* **2017**, *14*, 249–268. [[CrossRef](#)]
49. McFeeters, S.K. The use of the Normalized Difference Water Index (NDWI) in the delineation of open water features. *Int. J. Remote Sens.* **1996**, *17*, 1425–1432. [[CrossRef](#)]
50. Rasyid, A.R.; Bhandary, N.P.; Yatabe, R. Performance of frequency ratio and logistic regression model in creating GIS-based landslides susceptibility map at Lompobattang Mountain, Indonesia. *Geoenviron. Disasters* **2016**, *3*, 19. [[CrossRef](#)]
51. Mahdadi, F.; Boumezbear, A.; Hadji, R.; Kanungo, D.P.; Zahri, F. GISbased landslide susceptibility assessment using statistical models: A case study from Souk Ahras province, NE Algeria. *Arab. J. Geosci.* **2018**, *11*, 476. [[CrossRef](#)]
52. Banshtu, R.S.; Versain, L.D.; Pandey, D.D. Risk assessment using quantitative approach: Central Himalaya, Kullu, Himachal Pradesh, India. *Arab. J. Geosci.* **2020**, *13*, 219. [[CrossRef](#)]
53. Chen, W.; Fan, L.; Li, C.; Pham, B.T. Spatial prediction of landslides using hybrid integration of artificial intelligence algorithms with frequency ratio and index of entropy in nanzheng county, China. *Appl. Sci.* **2020**, *10*, 29. [[CrossRef](#)]
54. Weng, Q. *Remote Sensing and GIS Integration: Theories, Methods, and Applications*; McGraw-Hill: New York, NY, USA, 2010.
55. Devkota, K.C.; Regmi, A.D.; Pourghasemi, H.R.; Yoshida, K.; Pradhan, B.; Ryu, I.C.; Dhital, M.R.; Althuwaynee, O.F. Landslide susceptibility mapping using certainty factor, index of entropy and logistic regression models in GIS and their comparison at Mugling–Narayanghat road section in Nepal Himalaya. *Nat. Hazards* **2013**, *65*, 135–165. [[CrossRef](#)]
56. Zhao, X.; Chen, W. GIS-based evaluation of landslide susceptibility models using certainty factors and functional trees-based ensemble techniques. *Appl. Sci.* **2020**, *10*, 16. [[CrossRef](#)]
57. Zhao, X.; Chen, W. Optimization of computational intelligence models for landslide susceptibility evaluation. *Remote Sens.* **2020**, *12*, 2180. [[CrossRef](#)]

Disclaimer/Publisher’s Note: The statements, opinions and data contained in all publications are solely those of the individual author(s) and contributor(s) and not of MDPI and/or the editor(s). MDPI and/or the editor(s) disclaim responsibility for any injury to people or property resulting from any ideas, methods, instructions or products referred to in the content.